Comparison of catalytic activity of Co-Ni sulfide and Co-Ni sulfide/g-C_3N_4 nano-hybrids for overall water splitting

By

Rubab Zahra

School of Chemical and Materials Engineering

National University of Sciences and Technology

April 2021

Comparison of catalytic activity of Co-Ni sulfide and Co-Ni sulfide/g-C_3N_4 nano-hybrids for overall water splitting

Name: Rubab Zahra

Reg.No. 00000277401

This thesis is submitted as partial fulfilment of the requirements for the degree of

MS in Chemical Engineering

Supervisor Name: Dr Erum Pervaiz

School of Chemical and Materials Engineering (SCME)

National University of Sciences and Technology (NUST)

H-12 Islamabad, Pakistan

April 2021

Dedication

This thesis is dedicated to the seekers, willing to gain something in their lives.

Acknowledgements

First and foremost, I am grateful to **Almighty Allah**, who created; created man from the clot of congealed blood. Who taught man the use of pen, taught man that which he knew not.

I am in a debt of gratitude to my respected supervisor, **Dr Erum Pervaiz**, for believing in my abilities. Her incessant direction, encouragement and support were the driving force behind the success of this project. It was an honour working under her esteemed supervision and publishing a lot of data I have never thought.

I would like to encompass my sincere thankfulness to my worthy GEC members, **Dr Muhammad Bilal Khan Niazi** and **Dr Sarah Farrukh.**

The words are not in my command to compliment my loving parents, who have been my intellectual and spiritual inspiration. Their never-ending efforts and prayers sustained me at every stage of my life and invigorated me for attaining high goals. I can never forget to mention the great hustle created by **Mutawara Mahmood Baig** to complete my research work. **Dr Aftab Akram** for allowing me to complete my work in his lab. Lastly, I would like to pay my special thanks to my siblings, who are behind the scene editors. **Seerat Fatima, Asad Ali** and **Rida Fatima** thank you very much for understanding the load of this journey and doing my chores**. Zaara Ishaq, Atia Bano, Sara Ishaq and Farah-ul-Ain** your efforts for cheering me up and bearing me every day would be very much acknowledged. And last but not the least my lab mates **Maryum Ali** and **Osama Rabi** for understanding me and helping me out as much as possible. Deprived of this moral support, the thesis would have been much difficult.

Rubab Zahra

Table of Contents

Abbreviations

HER	Hydrogen evolution reaction
OER	Oxygen evolution reaction
GCN	Graphitic carbon nitride
CV	Cyclic voltammetry
LSV	Linear sweep voltammetry
XRD	X-Ray diffraction
IR	Current resistance
EDS	Energy-dispersive X-ray spectroscopy
SEM	Scanning electron microscopy
BET	Brunauer-Emmett-Teller
EIS	Electrochemical impedance study
ESCA	Electrochemical active surface area
C_p	Specific capacitance
R_{ct}	Charge transfer resistance
Ni	Nickel
Co	Cobalt
S	Sulfur
OCV	Open circuit voltage
NF	Nickel foam
Pt	Platinum

List of Figures

List of Tables

Abstract

Employing clean energy sources to produce hydrogen from the process of electrocatalytic water splitting has become one of the long-term solutions to the problems of depleting energy sources. To develop stable, efficient and non-noble electrocatalyst for water splitting is very crucial. Because of their low cost, pH stability and enhanced catalytic activity cobalt and nickel sulfide have become popular. But due to the problems of low surface area and higher over-potentials, the supplication of these sulfides is limited. To solve this problem different coupling techniques of these sulfides with highly active and porous materials have been employed.

Advancing highly stable and active bifunctional transition metal sulfide-based electrocatalyst for water splitting is essential for fuel cell technology and the production of hydrogen. Herein, a three-dimensional hierarchical electrocatalyst in the form of flower pattern, aligning graphitic carbon nitride sheets with cubic crystalline Ni-Co sulfide on a nickel foam support, is introduced as a bifunctional electrocatalyst with an outstanding performance. $CoNi_2S_4$GCN heterostructure prepared by using a hydrothermal method to extend g-C_3N_4 porous layers, developed in higher catalytic activity for oxygen evolution and hydrogen evolution reactions with overpotentials of 310 mV and 160 mV to afford a current density of 30 mA/cm^2 and 10 mA/cm^2. It is revealed that the astonishing features of this catalyst lie in the high porosity and surface area of conductive GCN support, the interfacial bonds between Carbon, nitrogen and cobalt, nickel sulfide and the three-dimensional configuration. The electrolyzer displays electrolysis at 1.58 V to reach a current density of 10 mA/cm^2 with long term durability of 24 hours. This approach of preparing $CoNi_2S_4$GCN leads to enhanced kinetics for OER/HER, more exposed surface area, faster electron transport, enhanced diffusion of electrolyte and opened a new path of enhancing the catalytic activity of water splitting reactions.

Chapter 1

Introduction

Due to the depleting resources, fossil fuels can no longer attain continuously escalating energy needs of mankind, therefore undoubtedly the hunt for renewable energy resources is the pressing priority [1]. The endowment of various sustainable energy technologies has grown considerably over the last few years. According to the figures from 2013, global energy demand reached 18 TW, 80% of which originate from natural energy resources (gas, coal and oil) [3]. The increase in global energy demand is anticipated to be 24 or 26 TW up till 2040, under the scenario of "new policies" or "current policies" accordingly. Also, the increase in carbon dioxide emissions is predicted to be 37 or 44 Gt/year in 2040, which was recorded to be 32 Gt/year in 2013. And all this is to happen because of the rapid population growth and increased industrialization. The situation seems quite alarming because of the increase in energy demand and supply and a drastic decrease in the sources responsible for its production. Given to this, the world is putting its thought and resources to develop energy systems which consume renewable energy sources (solar power, hydroelectric power and wind energy) for the sake of preservation of nature and climate.[2, 3] Owing to all these circumstances the world is focusing on the production of chemical fuels which are sustainable and are a much more natural and cheap resource of energy. For this, the industrial chemicals like methanol, ethylene, propylene, hydrogen, hydrogen peroxide, ammonia etc., could be used as a sustainable energy resource for the production of chemicals to make products needed worldwide on daily basis with reduced emission of CO_2 [4].

Hydrogen has been recognized as an auspicious renewable resource and is the most common element on earth. Besides hydrogen high energy density with zero emissions of byproducts that have an adverse environmental effect [5, 6]. Among various techniques for producing hydrogen, electrocatalytic water splitting has been known for the cleaner production of hydrogen [7]. The energy input of 237.1 $kJ.mol^{-1}$ with 1.23 V of potential is required for electrocatalytic water splitting. But actually to attain required current density this potential value increases from 1.23 V to 1.8-2.5V due to the complex kinetics of HER at cathode and OER at anode [7-9].

To overcome this problem noble metal electrocatalysts like platinum were used. Producing hydrogen by electrocatalytic water splitting technique still has some limitations of higher overpotentials and fundamentally slower kinetics taking place due to two half-cell reactions i.e. at the anode and the cathode [10]. Employing electrocatalytic water splitting for mass production of H_2 is suppressed because of the ineffective progress of HER in an acidic environment, higher overpotentials and sluggish dynamics of 4 electron transfer process in oxygen evolution reaction and lower durability of electrode materials [11]. The advanced catalysts used for OER are Ir and Ruthenium based oxides and platinum-based materials for HER [12]. Nevertheless, insufficiency and over the price of these noble metals have restricted their widespread use for large-scale industrial application. Hence, efforts are being made to design the innocuous and inexpensive electrocatalysts for using as highly active electrode materials for HER and OER is of great importance[13]. Various transition metals hybrids composed of oxides, sulfides, phosphides, carbides; nitrides have been reported as an efficient electrode for the application of water splitting [14-18]. Because of their low cost, enhanced electrocatalytic activity, thermal and mechanical durability; nickel and cobalt sulfides been recognized as promising electrode material for hydrogen production. They possess engrossing properties such as high conductivity, enhanced capacitance and outstanding reversibility for redox reactions [19-23]. Cobalt sulfide based electrocatalysts are regarded among the most efficient catalysts for water splitting. Still, their OER activity is very deficient [24, 25]. Cobalt sulfide with hybridized with metal ions such as nickel, copper or iron to adjust the electronic structure of cobalt sulfide and to increase their oxygen evolution reaction activity. Bimetallic nickel cobalt-based materials are believed to have efficient catalytic activity when compared with NiS and CoS [26]. Properties like enhanced conductivity and electrocatalytic activity are exhibited by nickel-based materials [27]. Nickel cobalt sulfide ($NiCo_2S_4$) has gained much importance as an electrocatalyst for HER because of its low cost, distinctive features and enhanced stability for a longer time [28, 29]. However, the higher resistance between powdered particles when comes in contact in a catalyst ink, limits its electrocatalytic activity. But there are many possibilities of improvements in the structure of nickel cobalt sulfide and to employ them as an efficient catalyst for electrocatalytic water splitting. Du et al. synthesized 3D shells of CoS on a nickel foam support with increased active sites for improved HER and OER activity [30]. Wang et al. designed $CoNi_2S_4$

under various temperature range that exhibited higher HER activity in alkaline media [31]. The electrocatalytic activity increases if $CoNi_2S_4$ is composited with various conductive substrates such as graphene and various transition metal nanosheets [32, 33]. Concerning this, graphitic carbon nitride was considered as an ideal candidate to increase the catalytic activity of various electrocatalysts for water splitting [34-36]. Li et al. used thermal polycondensation process for doping of g-C_3N_4 that enhanced the active sites of graphitic carbon nitride thus displaying outstanding HER performance in alkaline media [37]. Bhowmik et al. introduced CoFe hydroxide on g-C_3N_4 prepared by utilizing one pot co-precipitation method for enhancing the electrocatalytic performance of CoFe hydroxide with a electrolysis potential of 1.61 Volt to attain a current density of 10 mA/cm^2 for the overall water splitting [38].

Very few, work had been reported on graphitic carbon nitride and $CoNi_2S_4$ as a catalyst for the overall electrocatalytic water splitting. In this work, we utilized the hydrothermal technique to synthesize $CoNi_2S_4$ nanotubes on a g-C_3N_4 substrate. The experimental results have shown that the addition of g-C_3N_4 enhances the active surface area and contributes to enhancing the electronic conductivity of $CoNi_2S_4$. Three dimensional $CoNi_2S_4$/ g-C_3N_4@NF provided excellent electrolyte penetration and faster migration of oxygen and hydroxyl released during the overall water splitting to acquire current density of 10 mA/cm^2 and with an electrolysis potential of 1.58 Volt in an alkaline environment.

1.1 Characteristics of Cobalt sulfide

Unique physical and chemical properties are exhibited by transition metal cobalt sulfide. These sulfides play a significant role in the electrocatalytic features of hydrogen evolution reaction [39]. By employing various raw materials and by using different synthesis techniques these cobalt sulfides have shown diverse morphologies like layered, granular and rod-shaped. But properties like enhanced surface area and excellent conductivity are only depicted by nano-particles of cobalt sulfide. When compared with cobalt phosphide, cobalt sulfides have shown lower electrocatalytic activity, because the strong bond between hydrogen and sulfur atom, due to increased electronegativity of sulfide ion leads to higher over-potentials for electrocatalytic water splitting. These sulfides act as semi-conductor with reduced cost and great stability in an acid-base environment [40]. The addition of conductive substrate solves this problem of lower activity of cobalt sulfide [41]. Various crystalline forms of cobalt sulfide are found such as CoS_2, CoS, Co_3S_4, CoS_x, etc as shown in figure 1 [42]. Owing to its great stability in KOH electrolyte CoS_2 has tremendous applications in supercapacitors and batteries due to its high specific capacitance. The synthesis technique of these cobalt-based sulfides determines their electrochemical properties and applications [43].Cobalt sulfides have shown superior OER activity in alkaline electrolyte due to deficient dissociation of water and Volmer reactions taking place. Excellent OER and HER activities are depicted by Co_9S_8 in KOH electrolyte [44].

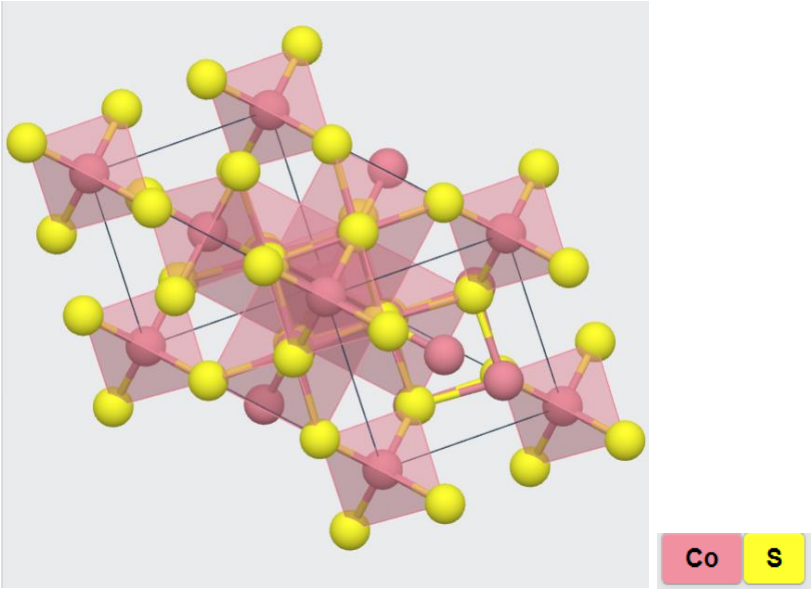

Figure 1. Co_3S_4 crystal structure

1.2 Characteristics of nickel sulfide

Nickel sulfide is found in various forms like Ni_3S_2, NiS_2, Ni_3S_4, NiS, etc. During the electrocatalytic oxygen evolution reaction, these transition metal sulfides are not stable and are easily changed into their relevant oxides. In an alkaline media, for hydrogen evolution reaction NiS_2 is stable and requires an over-potential of 67 mV [45]. Nickel sulfide has gained much importance among various transition metal sulfides because of its easy synthesis technique, high catalytic efficiency and reduced cost. The crystalline structure of NiS has been shown in figure 2. Depending on the method of preparation nickel sulfide is also available in various forms such as nanoparticles, sheets, etc. [46] Cobalt and nickel sulfide being the member of the same family of the periodic table almost exhibits same electrocatalytic activity. Ni_3S_2 has been known to exhibit best electrocatalytic activity among various other forms of nickel sulfide, following the trend as NiS < NiS_2 < Ni_3S_2 [46].

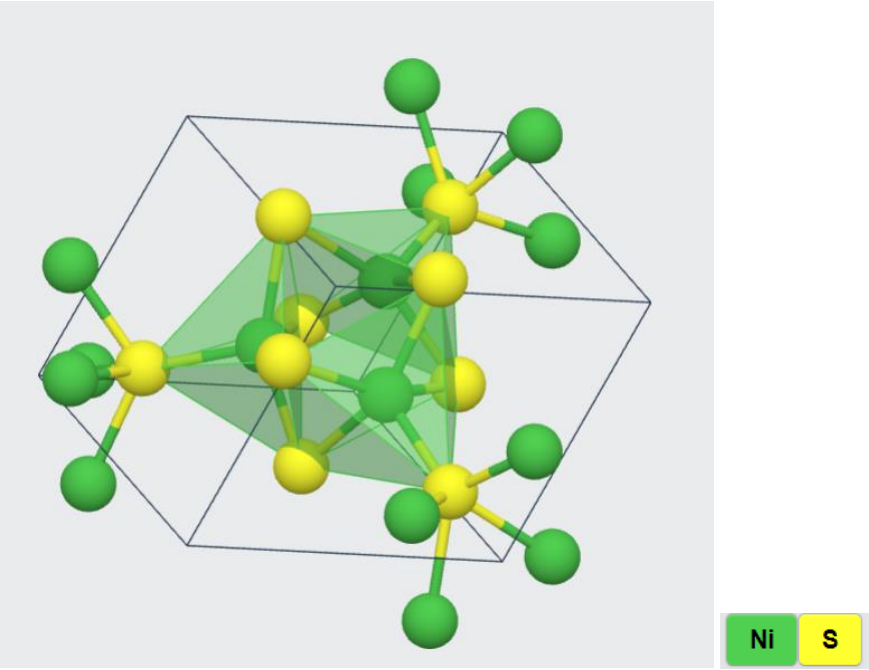

Figure 2. NiS crystal structure

1.3 The general mechanism for HER and OER

To gain knowledge about the mechanism of oxygen and hydrogen evolution reaction (HER) is crucial for a clearer picture of the reaction rate for overall water splitting. Electrolysis of water takes place in two half-reactions; cathodic hydrogen evolution reaction (HER) and anodic oxygen evolution reaction (OER) as revealed in figure 3. For the electrolysis of water, the thermodynamic potential required is 1.23 V under the reversible hydrogen electrode and +273 $kJmol^{-1}$ of Gibbs Free energy [47]. Hydrogen evolution reaction (HER) is greatly influenced by the pH conditions of the reaction and any change in pH of electrolyte results in poor HER kinetics. Alkaline water electrolyzer and polymer electrolyte water electrolyzer are mostly employed for electrocatalytic water splitting. But polymer-based electrolyte water electrolyzer has limited applications, as the only electrodes composed of noble metals exhibit stability. Alkaline water electrolyzer being used commercially exhibits great stability for non-precious metals [48].

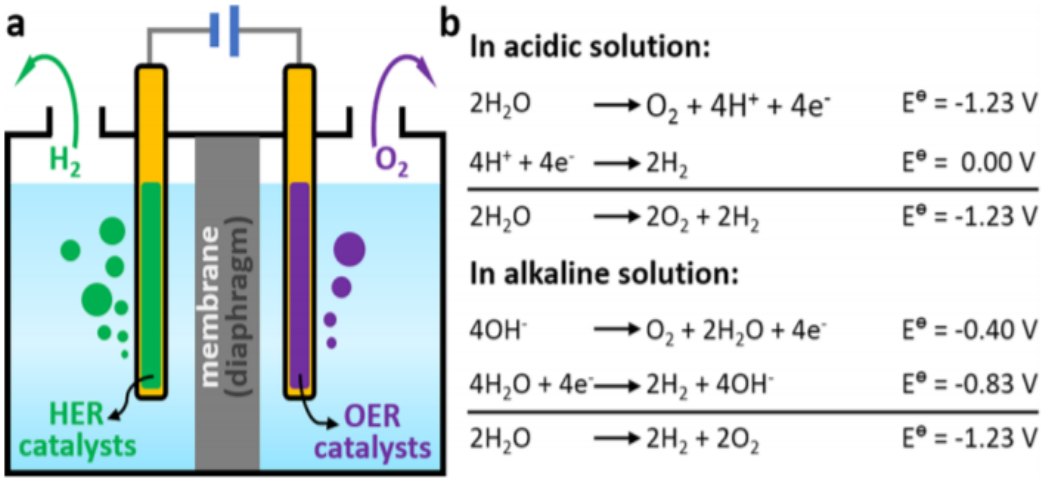

Figure 3. (a) Scheme of conventional water electrolyzers. (b) Water splitting reactions under acidic and alkaline conditions [7].

To gain insight into the HER mechanism in the acidic condition, using Volmer reaction, due to the fusion of electron and proton at the catalytic site, a hydrogen atom is generated [47]. In the Heyrovsky reaction, this generated hydrogen after combing with proton and electron produces hydrogen molecule and liberates the active site of a catalyst and then finally in the Tafel reaction, on the catalyst active site the two absorbed hydrogen atoms combines to yield hydrogen molecule. And the HER mechanism under basic conditions takes place with the combination of electron and water molecule to yield adsorbed hydrogen on the active site of a catalyst in the Volmer reaction, in Heyrovsky reaction, this adsorbed hydrogen merges again with the water molecule to yield hydrogen molecule and finally, the same process takes place in Tafel reaction as in the case of acidic conditions [47]. The overall potential of the cell for electrocatalytic water splitting is dependent upon the over-potential values, (created by the concentration difference of charges between the electrolyte and the electrode surface thus increasing the charge transfer resistance), the thermodynamic potential for electrolysis of water and ohmic losses [49]. The energy to favour such a complex reaction is obtained either by using an efficient electrocatalyst in an electrolyzer or from the renewable energy sources. The development of an electrocatalyst for water splitting is hindered by this high over-potential for HER at the cathode [49]. By employing an active catalyst on an electrode surface this problem of high over-potential is solved. The catalyst

employed for electrocatalytic water splitting lowers the activation energy thus providing active sites on the surface to adsorb hydrogen molecule and to stabilize the rate of charge transfer [50]. Based on Sabatier volcano plot, between current density and hydrogen binding Gibbs free energy it was revealed that nickel has shown enhanced catalytic activity for HER after previously used electrocatalyst for HER platinum [51]. Belonging to the same group of the periodic table, cobalt and nickel sulfides have been used as efficient HER catalysts, after integrating them with various materials.

To gain insight into the mechanism of oxygen evolution reaction (OER), this half-reaction of water splitting in alkaline media is demonstrated as:

$$C + OH^- \longrightarrow COH \quad (1.31)$$

$$COH + OH^- \longrightarrow CO + H_2O \quad (1.32)$$

$$2CO \longrightarrow 2C + O_2 \quad (1.33)$$

$$CO + OH^- \longrightarrow COOH + e^- \quad (1.34)$$

$$COOH + OH^- \longrightarrow C + O_2 + H_2O \quad (1.35)$$

Where CO and COH are the intermediates on the catalyst surface. OER for electrocatalytic water splitting is a heterogeneous reaction, in which the bond interactions between intermediates (COH, CO, COOH) are very important for the overall electrocatalytic activity of the catalyst. In the first step OH ion occupies the active sites of the catalyst to form COH intermediate, this intermediate again combines with hydroxyl ion to form oxygen atom which in the third step is converted to an oxygen molecule and liberates the active site of the catalyst [52]

1.4 Benchmarks for evaluation of the electrocatalytic activity

1.4.1 The selection of the counter electrode and the appropriate calibration of a reference electrode

To carry out HER measurements a three-electrode system is employed. Relative to the reference electrode working electrode's potential is measured. There are two methods to check the reference electrode before running the electrochemical experiments, first, is the cyclic voltammetry test calibrated for reversible hydrogen electrode which uses highly pure hydrogen is used as electrolyte and platinum as a counter electrode and the second is known as the cyclic voltammetry test of potassium ferri-cyanide in which KCl-$K_3Fe(CN)_6$ is employed as an electrolyte. The accuracy of the working electrode is calculated by comparing the redox potentials of Fe^{2+}/Fe^{3+}. Platinum used as a counter electrode cannot be used under acidic conditions.[53]

1.4.2 Onset over potential and Over-potential for HER and OER

Onset over-potential is defined as the initial point where the current starts to rise and is calculated from the LSV diagram. The further potential to lead the chemical conversion up to a specific rate is known as over-potential. It is generally calculated at 10 mA/cm^2 of current density, from the following equation:

$$E_{electrolysis} = E_{irreversible} + IR + \Delta E_{irreversible} \quad \text{(Eq. 1)}$$

$E_{reversible}$ is the decomposition voltage

IR is the voltage drop by electrolyte, wires

And $\Delta E_{irreversible}$ is over-potential for hydrogen evolution reaction

Over-potential is resulted by the polarization due to concentration and electrochemical opposition. IR losses are reduced by placing electrode face closer to the tip and the electrochemical opposition is reduced by employing efficient HER electrocatalysts. An ideal electrocatalyst for overall water splitting gives high current density with low over-potential values but the high capacitive current is produced by

electrocatalysts having a high electrocatalytic active surface area (ESCA) that can be reduced by employing low sweep rates in the linear sweep voltammetry (LSV) [53].

1.4.3 Electrochemical impedance spectroscopy (EIS)

To study the HER kinetics and to understand electrolyte/electrode interaction reaction electrochemical impedance spectroscopy (EIS) is done. Current is measured after applying an alternating current voltage of various frequencies during EIS measurements. The resistance in Ohms law is known as the impedance in EIS. A Nyquist plot is formed as a result of the frequency response to AC impedance. Nyquist plot figure is a semicircle between real v/s imaginary impedance. Charge transfer resistance denoted by R_{ct} is attained from the semicircle diameter in high-frequency regions. And adsorption resistance of intermediates adsorbed on the surface of the electrode is obtained from semicircle in low-frequency regions. The smaller diameter of this semicircle depicts smaller R_{ct} value and more rapid reactions. EIS study is done after the electrochemical cell stabilizes under open-circuit voltage (OCV) conditions.

1.4.4 Tafel slope and the exchange current density

The value of the Tafel slope gives further information about the reaction kinetics and is obtained from the LSV curves, directly from the electrochemical workstation or from the impedance report. A voltage applied for the calculation of Tafel slope is same as the polarization curves. From the LSV plot, this Tafel slope is calculated by plotting the log of current density v/s overpotential for HER or OER and then from the slope of this plot Tafel slope value is gained, from the following Tafel equation [8];

$$\eta = b.\log j + a \qquad \text{(Eq. 2)}$$

Where, η = over-potential, b = Tafel slope, j = current density

Tafel slope is calculated from the impedance report by plotting linear fit of charge transfer resistance and over-potential [54]. The value of exchange current density is

highly dependent upon the type of electrolyte, temperature and on the electrode surface, higher values of this current density depict advantageous HER and OER kinetics.

1.4.5 Stability (Chronopotentiometry or Chronoamperometry)

To commercialize an electrocatalyst for overall water splitting the most important parameter is its durability. To examine this stability of an electrocatalyst chronopotentiometry, chronoamperometry and cyclic voltammetry are done. CV is used to measure the current of an electrode under an applied voltage. And after running 1000 and above CV cycles polarization curve is compared with before running CV cycles LSV curve to check the stability of an electrode. In chronoamperometry change in the current while applying fixed potential is recorded for a longer period to check the stability of electrode in an electrolyte. These techniques are used to gain insight into redox reactions. [8]

Chapter 2

Literature review

All the latest developments are done in nickel and cobalt sulfides and their hybrids for overall water spitting are done by either morphological and structure tuning to enhance the electrocatalytic activity of the sulfides or by employing cobalt and nickel sulfide together or with various active materials that increase their catalytic activity for water splitting. By now, employing nickel foam in place of conventionally used glassy carbon electrode reduces degradation problems in the acidic environment. Nickel sulfide together with its various alloys like Lanthanum-Nickel-Aluminium/Nickel sulfide has revealed increased HER activity. The benefit of metal-organic frameworks (MOFs) has also been known to enhance the overall activity for electrocatalytic water splitting. Tuning with these features of transition metal sulfides enhances their intrinsic and extrinsic properties.

2.1 Hybrids with various metals

The alloy of nickel sulfide has been recognized as an efficient HER catalyst, but during the electrocatalytic water splitting process this alloy drops off its catalytic activity. Because of their property to avoid disintegration of the electrode under OCV condition and their vigorous adsorption strength, hydrogen-producing alloys have become popular like hydrogen alloys of AB_5 type have shown excellent catalytic activity in alkaline media [55] but the decomposition of the electrode, hinders their development. Most of the work has been done on Lanthanum-Nickel-Aluminium/Nickel sulfide alloy, Ni-Fe alloy embedded in carbon, Cobalt tungsten sulfide and nickel tungsten sulfide, cobalt iron sulfide with carbon nanotubes [56] [57] [58].

2.2 Hybrids on a durable support

Synthesizing an electrocatalyst directly on durable support increases electron/ion transport rates and eliminates the use of any binder because polymer binders block the active sites of the catalyst [59]. Peng et al. have employed 3D CoS_2/Reduced Graphene Oxide-Carbon Nano Tubes as HER catalyst.[60] Cobalt sulfide on graphene was prepared by simple hydrothermal method and by vacuum filtration carbon nanotubes were added to the above solution. Cobalt sulfide sheets align vertically on the graphene, as seen from the TEM results. XRD showed that there was no diffraction peak of reduced graphene oxide. XPS also revealed the purity of CoS_2. Raman spectroscopy confirmed the presence of RGO. For CoS_2/Reduced Graphene Oxide-Carbon Nano Tubes electrode higher concentration of CNT gives higher bendability. SEM images showed that the composite CoS_2/RGO was wrapped and distributed uniformly over porous CNT. TEM images confirmed the good mixing of composite with CNT sheet. From LSV curves, it was revealed that CoS_2/Reduced Graphene Oxide-Carbon Nano Tubes had lower over-potential when compared with cobalt sulfide on reduced graphene oxide. In acidic media these CNT have little HER activity [60]. The current density of CoS_2/Reduced Graphene Oxide-Carbon Nano Tubes was also enhanced. Due to the sheet-like structure of this hybrid, it has more active sites available for hydrogen absorption resulting in an increased HER activity. CoS_2/Ti composite grown on a nickel foam has shown enhanced catalytic activity [61].

2.3 Hybrids for universal pH application

Most of the electrocatalysts for water splitting cannot be employed in an acidic electrolyte that hinders their development. Progress in developing compatible electrocatalysts for neutral pH applications are being made to lessen the environmental burden. Cobalt-based catalysts supported on poly-pyridine ligand exhibit increased HER performance in water electrolysis [62, 63]. It was investigated that electrodeposited cobalt sulfide films acted as an efficient HER catalyst in aqueous media and maintained stability for 40 hours in neutral pH

water [39]. Tang et al. have synthesized nickel sulfide directly grown on a carbon cloth employing hydrothermal method [64]. From the cyclic voltammetry results of this electrode, it was revealed that this hybrid had enhanced HER activity, extremely high double-layer capacitance C_{dl} of 5.7 mF/cm^2 and enhanced current density. From the data of LSV curves, the over-potential of NiS_2 NA/CC is far less than bare nickel sulfide.[64] 3D graphene on nickel foam synthesized by chemical vapour deposition method showed interesting properties like stability, low density, flexibility and good conductivity [65].

2.4 MOFs based cobalt and nickel sulfide

Owing to their porous framework and stable support to enhance electrocatalytic activity and electrocatalytic active surface area metal-organic frameworks (MOFs) have gained traction. Because of their eccentric properties like varying structure and adjustable functions, ZIFs a type of MOF has gained popularity. Transition metal sulfides derived from metal-organic frameworks and with carbon encapsulated in them are unique [66]. Chen et al. have worked on nickel substituted cobalt sulfide derived from ZIF67 and incorporated in nitrogen-doped carbon and sulfur. This hybrid has revealed excellent catalytic activity for OER because of that nickel replacement [67]. Zhang et al. have reported that three-dimensional zinc-cobalt-sulfide can be prepared by solvent sulfidation technique on a ZIF template [68]. The composite depicted increased ESCA, enhanced conductivity and excellent durability in alkaline media. Polarization curves for this composite showed low over-potential and smaller Tafel slope values, thus depicting the enhanced electrocatalytic activity of Cobalt-based MOF for the application of water splitting [68].

2.5 The combined function of nickel and cobalt sulfide

The fusion of nickel and cobalt sulfide has been known by several authors to enhance their electrocatalytic activity. Cui et al. employed a hydrothermal method to synthesize Cobalt sulfide sheets with various doping of nickel to enhance the overall activity of the catalyst [69]. From the electrochemical study,

this composite with doping of only 10% revealed lower overpotential and excellent durability after 3500 Cyclic voltammetry (CV) cycles in acidic electrolyte. Density functional theory (DFT) calculations further confirmed the suitable kinetics for producing hydrogen from water by employing Nickel doped cobalt sulfide electrode. The increased electrocatalytic activity of the hybrid was also contributed to the low energy barrier of 0.21 eV [69]. Jiang et al. have synthesized

Nickel cobalt sulfide in a hollow sphere by employing a solvothermal method to enhance its electrocatalytic activity [70]. Results of BET analysis, it was seen that $NiCo_2S_4$ BHSs showed the highest BET surface area among various other catalysts. Besides $NiCo_2S_4$ BHSs revealed the smallest value of onset over-potential among various other catalysts and as compared to another base-metal sulphide $NiCo_2S_4$ BHSs depicted great HER activity in alkaline electrolyte. The inclusion of cobalt on transition metals increases their electrocatalytic activity because of the decrease in the free energy of intermediates [71]. Liu et al. have worked on nickel-cobalt-molybdenum sulfide incorporated on nickel foam with an interwoven nano-sheet like structure [72]. This interwoven nano-sheet composite has shown reduced overpotential as revealed from its LSV curves because of its unique structure. Double-layer capacitance calculated from cyclic voltammetry in non-faradic regions has shown enhanced surface area of this composite which was another reason behind high catalytic activity [72].

Table 1: Compared electrocatalytic activity of various materials for hydrogen evolution reaction

Hybrids	**Supported on**	**Tafel slope ($mV.dec^{-1}$)**	**Over Potential HER (mV)**	**Current density ($mA.cm^{-2}$)**	**Reference**
Lanthanum Nickel-Aluminium/Nickel Sulfide alloy	Nickel wire	121	70	100	[73]
Ni–Fe-C	A3 steel	-	65	20	[58]
Nickel tungsten sulphide	Carbon electrode	96	340	5	[57]
Cobalt tungsten sulphide	Glassy carbon electrode	78	238	5	[57]
Cobalt sulfide films	F-doped tin Oxide electrode	93	43	50	[39]
Ni_3S_2/Ni foam	Nickel foam	108	220 and 396	10 and 100	[74]
CoS_2/Reduced graphene oxide and carbon nanotubes	RGO	51	142	10	[60]
CoS_2/Tin foil	Ti foil	72	81	12.37	[61]
$CoNi_2S_4$ nanorod	Carbon electrode	53	111	10	[75]
$CuCo_2S_4$ cluster	Carbon electrode	63	135	10	[75]
CoS_x/Ni_3S_2@ NF	Nickel foam	133	280	20	[19]

Hybrids	**Supported on**	**Tafel slope ($mV.dec^{-1}$)**	**Over Potential HER (mV)**	**Current density ($mA.cm^{-2}$)**	**Reference**
Cobalt molybdenum sulfide-H	Glassy carbon electrode	89	122	10	[76]
Nickel cobalt molybdenum sulphide nano-boxes	Glassy carbon electrode	51	125	10	[77]
Ni_1Co_4S@C-1000	ZIF-67	64	1430 for OER	10	[67]
Ni_1Co_4S@C-800	ZIF-67	112	247 for HER	10	[67]
Nickel cobalt sulphide -3	(flourine doped tin oxide)	93 and 70	280	10	[78]
$Co_{0.9}Ni_{0.1}S_2$	Glassy carbon electrode	52	156	10	[69]
$NiCo_2S_4$ BHSs	Glassy carbon electrode	60.4	90	0.275	[70]
$NiCo_2S_4/Ni_3S_2$/NF	Nickel foam	105.2	600	600	[79]

Chapter 3

Materials and methods

3.1 Materials

Melamine, Sodium Sulfide Nonahydrate ($Na_2S.9H_2O$), cobalt nitrate hexahydrate, nickel nitrate hexahydrate, hexamethylenetetra amine (HMT), were purchased from Sigma-Aldrich Co. Ltd. DI water was used in all experiments.

3.2 Synthesis of g-C_3N_4

Melamine was used to produce graphitic carbon nitride according to the previous reports [80, 81]. 10 gram of melamine was placed in a crucible and heated for 5 hours at 500^0C at a heating rate of 5^0C/min in a muffle furnace. The resulted yellowish powder was g-C_3N_4 used in this work

3.3 Synthesis of NiS and Co_3S_4

NiS was prepared by utilizing a simple hydrothermal method. Typically, 1.746 gram of nickel nitrate hexahydrate and 0.616 gram of HMT was added in 40 ml deionized water and 20 ml ethanol under continuous stirring for 30 minutes. Then, the precursor was transferred into a Teflon lined autoclave and kept at 180^0C for 6 hours. The green-coloured precursor was washed with DI water and ethanol and was dried at 70^0C for 10 hours. After that 0.5 gram of Sodium Sulfide Nonahydrate and the above precursor were added in 70 ml DI water under continuous stirring for 30 minutes and was then transferred into a hydrothermal autoclave and kept at 180^0C for 6 hours. The black-coloured NiS was obtained after repeating the above steps of washing and drying. Co_3S_4 was obtained using the above method except nickel nitrate hexahydrate was replaced by cobalt nitrate hexahydrate.

3.4 Synthesis of $CoNi_2S_4$ and $CoNi_2S_4$/g-C_3N_4

$CoNi_2S_4$GCNx was also prepared by a simple hydrothermal method. Typically, g-C_3N_4 **x** (x=30,50 and 100 mg) was added in 40 ml DI water and 20 ml ethanol. The solution was sonicated for 4 hours to obtain homogeneous g-C_3N_4 nanosheets. Then 1.164 gram of cobalt nitrate hexahydrate, 0.582 gram of nickel nitrate hexahydrate and 0.616 gram of HMT was added in the above solution under continuous stirring for 30 minutes. The precursor was transferred into a Teflon lined autoclave and kept at 160^0C for 12 hours. The obtained cobalt nickel oxide precursor was then washed DI H_2O and ethanol for various times and dried at 70^0C for 10 hours. After that 0.5 g of Sodium Sulfide Nonahydrate and the above precursor were added in 70 ml DI H_2O under stirring for 30 minutes and was then transferred into a hydrothermal autoclave and kept at 160^0C for 12 hours. The black-coloured composite was obtained after repeating the above steps of washing and drying. $CoNi_2S_4$ was synthesized using the same method without the addition of g-C_3N_4. The entire process has been illustrated in figure 4.

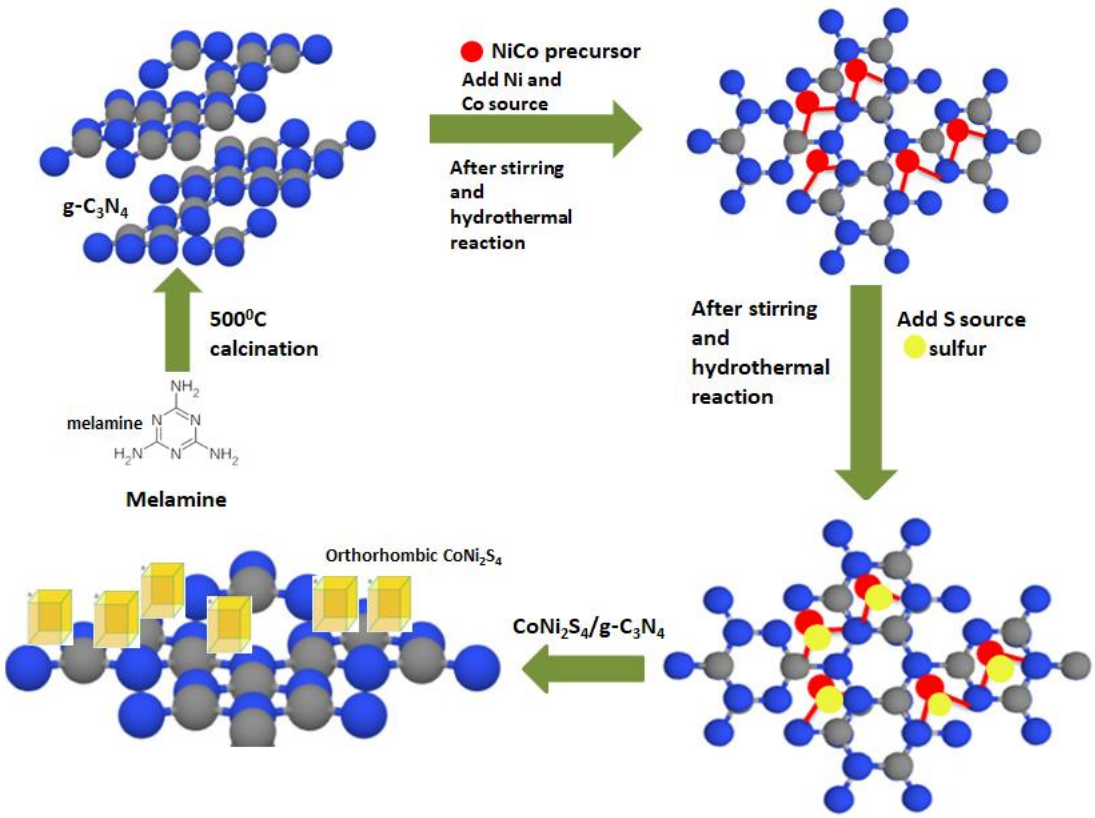

Figure 4. Schematic figure of the experimental procedure of $CoNi_2S_4$/GCNx.

3.5 Chapter-Characterization Techniques

The as-synthesized electrodes were analyzed by X-ray diffraction(STOE-Seifert X'Pert PRO), using 2θ values from 20^0 to 70^0 using Cu-Kα radiation for the determination of the crystallographic structure of as-synthesized materials. Scanning electron microscopy (JEOL-instrument JSM-6490A) equipped with an EDX was used to study the structure/morphology of the prepared materials. The Raman spectroscopy of the sample was done using a Model Raman spectrometer with a wavelength of 514 nm by Argon ion laser as excitation wavelength to determine the vibrational modes and any change in the bandwidth/ shift of all prepared samples. The pore structure and obtained surface area of the composite sample were measured by BET (Quantachrome, Virginia, USA), at 130^0C for 5 hours sample was degassed.

3.6 Electrochemical Characterization

The electrochemical tests for OER and HER were run on a Biologic workstation equipped with three-electrode assembly. The reference and counter electrodes were Ag/AgCl and Pt mesh. The ink for working electrode was prepared by the addition of 2 mg of active material, 20 µL of Nafion and 80 µL of ethanol under sonication for 4 hours with a 3.3 mg/cm^2 mass loading of catalyst on pre-treated nickel foam (1×1 cm) which was then dried at 80^{0}C for 2 hours. After drying the coated nickel foam (NF) was pressed under a pressure of 10 MPa using a hydraulic press. The catalytic activities of all electrodes have been analyzed in 1 M KOH solution using a three-electrode assembly at a scan rate of 5 mV s^{-1}. For simplicity, reversible hydrogen electrode potential was used for further calculations, which was obtained by the following equation:

$E_{RHE} = E_{Ag/AgCl} + 0.059pH + 0.1976$ (Eq. 3)

With pH = 14, for KOH solution. All the data of electrochemical measurement is balanced by the ohmic potential drop (iR). The Tafel slope for OER and HER is calculated from the equation [19]

$\eta = a + b \log j$ (Eq. 4)

Over potential was calculated according to the following equations:

Hydrogen evolution reaction, $\eta = 0 - E$ vs R (Eq. 5)

Oxygen evolution reaction, $\eta = 1.23 - E$ vs R (Eq. 6)

Besides, electrochemical impedance spectroscopy was done at a frequency range of 200 kHz-100 MHz, by providing a 10 mV alternating voltage amplitude. The stability of the as-prepared electrocatalysts was analyzed by chronoamperometry results.

Chapter 4

Results and discussion

4.1 Characterizations

4.1.1 X-ray diffraction (XRD)

To find out the crystalline structure and phase of all synthesized materials XRD study was done with the results shown in figure 5 (a, b). The XRD of nickel-cobalt sulfide structure in figure 1a, has shown characteristic peaks at 26.66^0, 31.47^0, 32.90^0, 38.16^0, 47.20^0, 50.25^0, 55.00^0, 57.71^0, 58.68^0, 64.77^0, 65.59^0, 68.99^0 , that referred to crystal plane of (220), (311), (222), (400), (422), (511), (440), (531), (620), (533), (622), (444). The cubic $CoNi_2S_4$ structure has a cell dimension of $a_0=b_0=c_0=9.47$, in which a and b sites are occupied by Co and Ni and c-site by S (JCPDS No. 00-024-0334). The diffraction peak of g-C_3N_4 appeared at 27.4^0 correspondings to diffraction plane of (002) [82]. Whereas, the XRD of $CoNi_2S_4$GCN (30, 50, 100) as revealed in figure 1b, all the diffraction peaks successfully manifested to cubic $CoNi_2S_4$ (JCPDS No. 00-024-0334). There is no obvious diffraction peak for g-C_3N_4 in GCN (30, 50) catalysts which might be due to lower g-C_3N_4 content and the surface was covered by $CoNi_2S_4$ nano-sheets, but a small peak of g-C_3N_4 is indicated in $CoNi_2S_4$GCN100 which might be due to higher graphitic carbon nitride content in this catalyst. The intensity of the peaks of g-C_3N_4 became weaker in $CoNi_2S_4$GCN50 indicating that there are rich defects in graphitic carbon nitride[83].

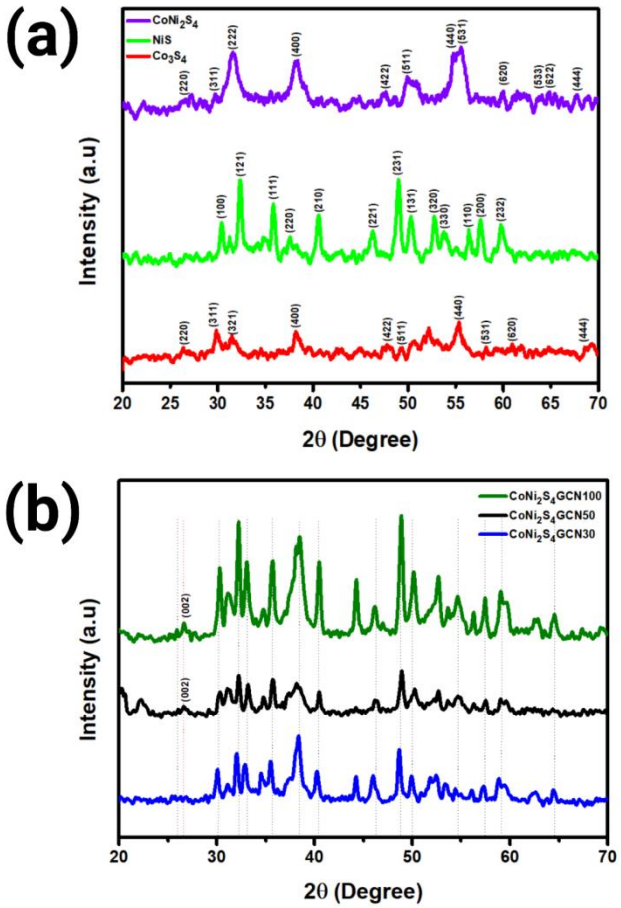

Figure 5. XRD spectrum of (a) Co_3S_4, NiS, $CoNi_2S_4$ and (b) $CoNi_2S_4$GCN30, $CoNi_2S_4$GCN50, $CoNi_2S_4$GCN100 catalysts

4.1.2 Raman Spectroscopy

Raman spectroscopy is performed to characterize the successful fabrication, chemical states and structural defects of $CoNi_2S_4$GCN composites. Raman spectra of $CoNi_2S_4$GCN composites are shown in figure 6. Raman spectra of pure g-C_3N_4 demonstrate peaks in the region of 1400 and 1564/cm [84, 85]. The as-prepared $CoNi_2S_4$GCN composites have shown sharp Raman peaks in the area from 100 to 500/cm in which vibrational modes of $CoNi_2S_4$ and D, G and 2D bands of graphitic carbon nitride could also be observed in 1200 to 1600/cm region. $CoNi_2S_4$GCN composites have shown Raman peaks of $CoNi_2S_4$ in the magnified 100 to 400 cm^{-1} region at 160, 255, 310 and 344/cm [86, 87]. Raman

peak around 2100/cm is due to the formation of a 2D band formed due to the lattice vibrations of two phonons in the carbon-based materials and the position of this band identifies several graphite layers which are consistent with the previous reports[88]. The 2D band of $CoNi_2S_4GCN$ composites is around 2100/cm lower than that of typical graphite 2703/cm indicating reduced number of graphite layers due to the exfoliation of g-C_3N_4 during sonication for 4 hours.

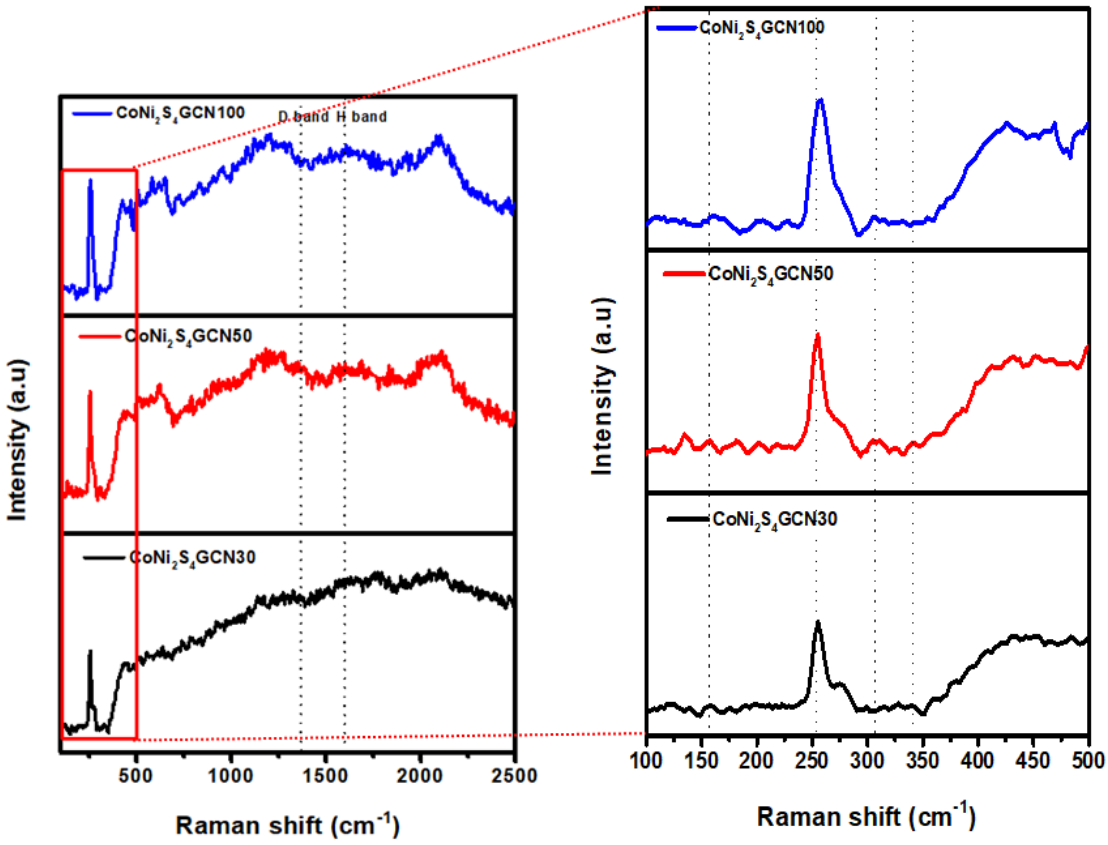

Figure 6. Raman analysis of $CoNi_2S_4GCN30$, $CoNi_2S_4GCN50$ and $CoNi_2S_4GCN100$ nanocomposites

4.1.3 Scanning Electron Microscopy (SEM)

The SEM of NiS as shown in Figure 7a has well-defined nano-rods with a diameter of 80 nm formed at 180^0C. These interconnecting rods are responsible for electrolyte penetration. Co_3S_4 in figure 7b has also shown nano-rods like structure with a diameter of about 75 nm but there are several agglomerates in the structure which are responsible for the lower surface area of this sample. SEM image of $CoNi_2S_4$ depicts a spherical flower-like pattern with a slight

agglomeration. The diameter of this sphere is around 114 nm and this petal-like pattern benefit the increase of the surface area. However serious agglomeration is still a problem in $CoNi_2S_4$. The addition of g-C_3N_4 as depicted in figure 7(d-f) have defined the structure of $CoNi_2S_4$ and resolved the problem of agglomeration. The well-defined spherical flower petals of $CoNi_2S_4$GCN50 have enhanced the surface area with more interconnecting layers of g-C_3N_4 and have increased the exposure of active sites of $CoNi_2S_4$. The higher catalytic performance of $CoNi_2S_4$GCN50 is exhibited by this petal-like highly aligned composite structure.

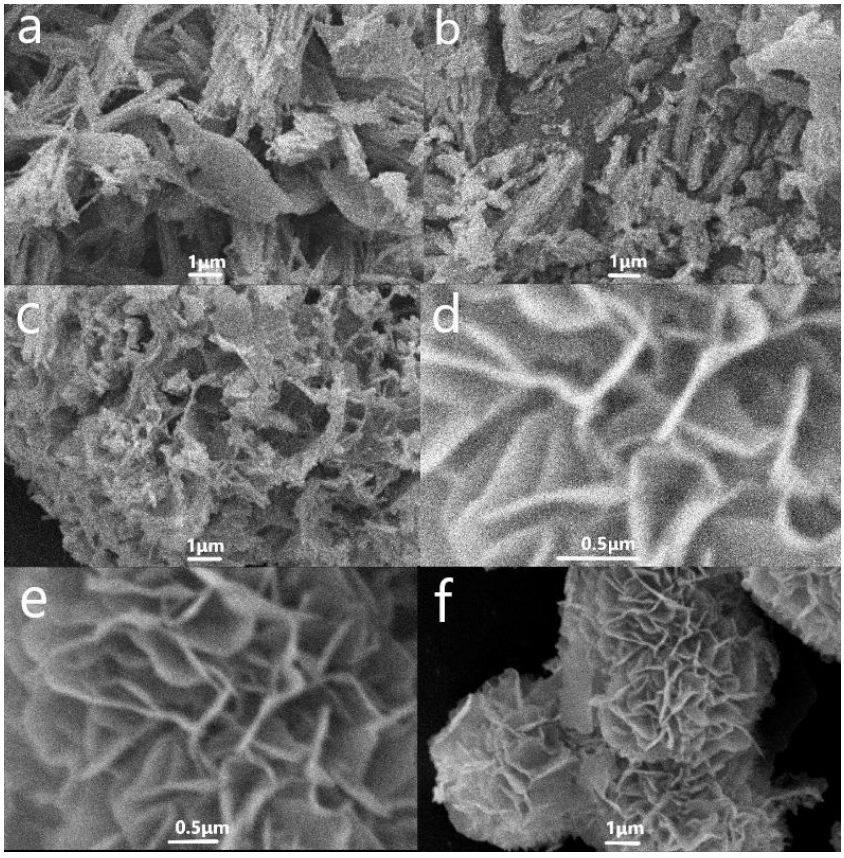

Figure 7. SEM images of (a) NiS ,(b) Co_3S_4 ,(c) $CoNi_2S_4$ and (d-f) $CoNi_2S_4$GCN50 at different magnifications.

4.1.4 Energy-dispersive X-ray spectroscopy (EDS)

In figure 8, the Energy-dispersive X-ray spectroscopy indicates the composite $CoNi_2S_4$GCN50 has a uniform distribution of elemental S, Co, Ni, N, C and O.

The higher concentration of S, Co, Ni, N and C reveals the successful fabrication of $CoNi_2S_4$ on g-C_3N_4 substrate. Their atomic percentage is shown in table 2.

Table 2: EDS of $CoNi_2S_4$GCN50

Element	**Weight %**	**Atomic %**
C K	20.52	36.07
N K	2.47	3.73
O K	28.66	37.83
S K	16.79	11.06
Co K	23.16	8.30
Ni K	8.39	3.02
Totals	100.00	

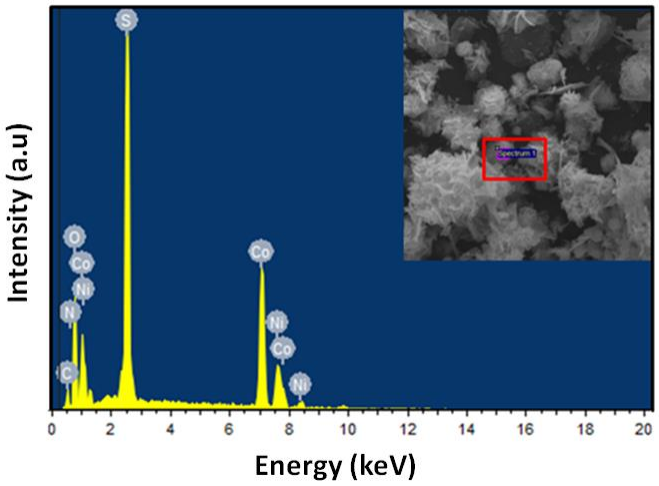

Figure 8. EDS of $CoNi_2S_4$GCN5

4.1.5 BET analysis

The BET (nitrogen adsorption-desorption isotherms) of $CoNi_2S_4GCN50$ are shown in fig.9. From these curves, the composite has shown hysteresis loop at high P/P_0 demonstrating type IV isotherms curve. $CoNi_2S_4GCN50$ composite has shown meso –macropores for efficient the transport of electrolyte to the sides of active layers as depicted from BET results. From the previous reports, $CoNi_2S_4$ has a microporous structure with S_{BET} of 3.5 m^2g^{-1} [89]. In the $CoNi_2S_4GCN50$ composite small amount of meso-macropores of g-C_3N_4 and more micropores of $CoNi_2S_4$ obtained from stacking of porous graphitic carbon nitride layers between nickel-cobalt sulfide have resulted in enhanced surface area of this electrocatalyst with an S_{BET} of 11.6121 m^2g^{-1} and a pore volume of 0.0528 cm^3g^{-1}. Thus the incorporation of graphitic carbon nitride efficiently increases the surface area and enough redox reactions at $CoNi_2S_4$ electrocatalyst.

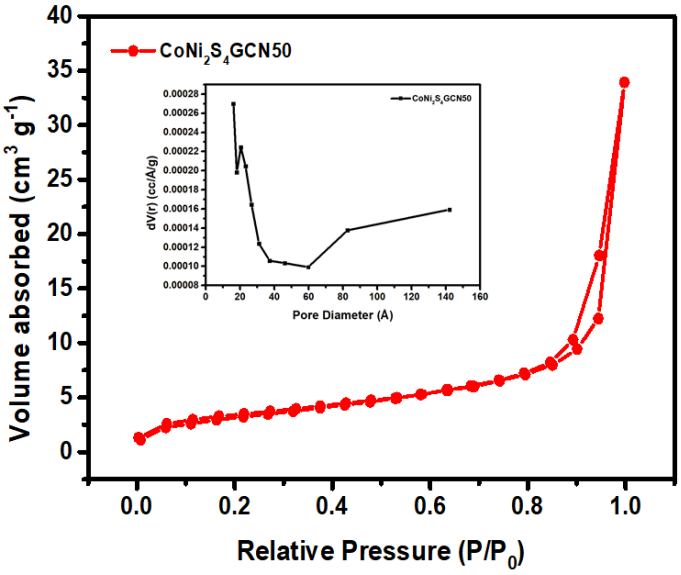

Figure 9. Nitrogen adsorption-desorption isotherms and pore size distribution of $CoNi_2S_4GCN50$

4.1.6 Electrochemical Characterization

4.1.6.1 Oxygen evolution reaction

To demonstrate the electrocatalytic activity of all the prepared catalysts towards OER, three-electrode assembly of Pt mesh, Ag/AgCl, NiS/NF, Co_3S_4/NF, $CoNi_2S_4$/NF, $CoNi_2S_4$GCN30/NF, $CoNi_2S_4$GCN50/NF and $CoNi_2S_4$GCN100/NF in 1M KOH electrolyte was used. For comparison, bare Ni-foam was also tested in 1 molar KOH solution. The OER activity of as-prepared catalysts was assessed through its LSV. Figure 10a, represent the LSV curves for OER of all samples, the polarization curve of $CoNi_2S_4$, $CoNi_2S_4$GCN30, $CoNi_2S_4$GCN50 and NiS exhibited oxidation peaks at ~1.38 V, ~1.35 V and 1.45V (vs RHE) because of the oxidation of Ni(2) to Ni(3) and Co(2) to Co(3) [90]. The anodic current density of $CoNi_2S_4$GCN50 increases quickly after 1.5 V. Linear sweep voltammetry reveals a great difference in the OER activities of all electrocatalysts. To avoid the effect of oxidation peaks of all samples on the current density, over-potential is taken at 30 and 100 mA/cm^2. As shown in fig. 10d the overpotential required for $CoNi_2S_4$GCN50 to reach a current density of 30 mA/cm^2 is 310 mV lower than $CoNi_2S_4$GCN30 (340 mV), $CoNi_2S_4$ (340 mV) and $CoNi_2S_4$GCN100 (350 mV) and NF (480 mV). $CoNi_2S_4$ (340 mV) even has a lower overpotential than NiS (380 mV) and Co_3S_4 (410 mV) at 30 mA/cm^2, depicting the influence of the combined effect of Ni and cobalt sulfide. LSV of graphitic carbon nitride on nickel foam is revealed in figure 11. The OER catalytic activity of $CoNi_2S_4$GCN50 is nearly equal to RuO_2@NF (300 mV at 30 mA/cm^2) [19] and various other electrocatalysts reported previously as depicted in table 3. The improved OER activity of $CoNi_2S_4$GCN50 electrocatalyst may be due to the synergistic coupling of Ni and Co with C and N. The addition of g-C_3N_4 lowers the affinity of active sites of Co and Ni and leads to adsorption binding energy of Nickel and cobalt to the intermediates (oxygen and hydroxyl molecule). g-C_3N_4 allows equilibrium coverage of intermediates on $CoNi_2S_4$ active sites and this porous network is responsible for enhanced diffusion of ions. Adding 30 mg of graphitic carbon nitride has almost no influence in enhancing the OER activity of $CoNi_2S_4$. Higher concentrations of g-C_3N_4 blocks the active sites and causes agglomeration of $CoNi_2S_4$, decreasing its electrocatalytic activity. $CoNi_2S_4$GCN50 has lowest over-potential for OER among the various as-prepared catalysts. Another standard to estimate the reaction kinetics for oxygen evolution

reaction is the Tafel slope shown in figure 10c, $CoNi_2S_4$GCN50 has shown the lowest Tafel slope (49.86 $mVdec^{-1}$) than $CoNi_2S_4$ (93.35 $mVdec^{-1}$), $CoNi_2S_4$GCN30 (93.21 $mVdec^{-1}$), $CoNi_2S_4$GCN100 (109.01 $mVdec^{-1}$), NiS (113.52 $mVdec^{-1}$), Co_3S_4 (121.50 $mVdec^{-1}$) and Ni foam (167.21 $mVdec^{-1}$). From the values of Tafel slope, the RTD (rate-determining step) as predicted is the "1st-electron transfer step" as:

$$EC + OH^- \longrightarrow EC\text{-}OH + e^- \qquad \text{Eq. (7)}$$

Where EC stands for electrocatalyst.

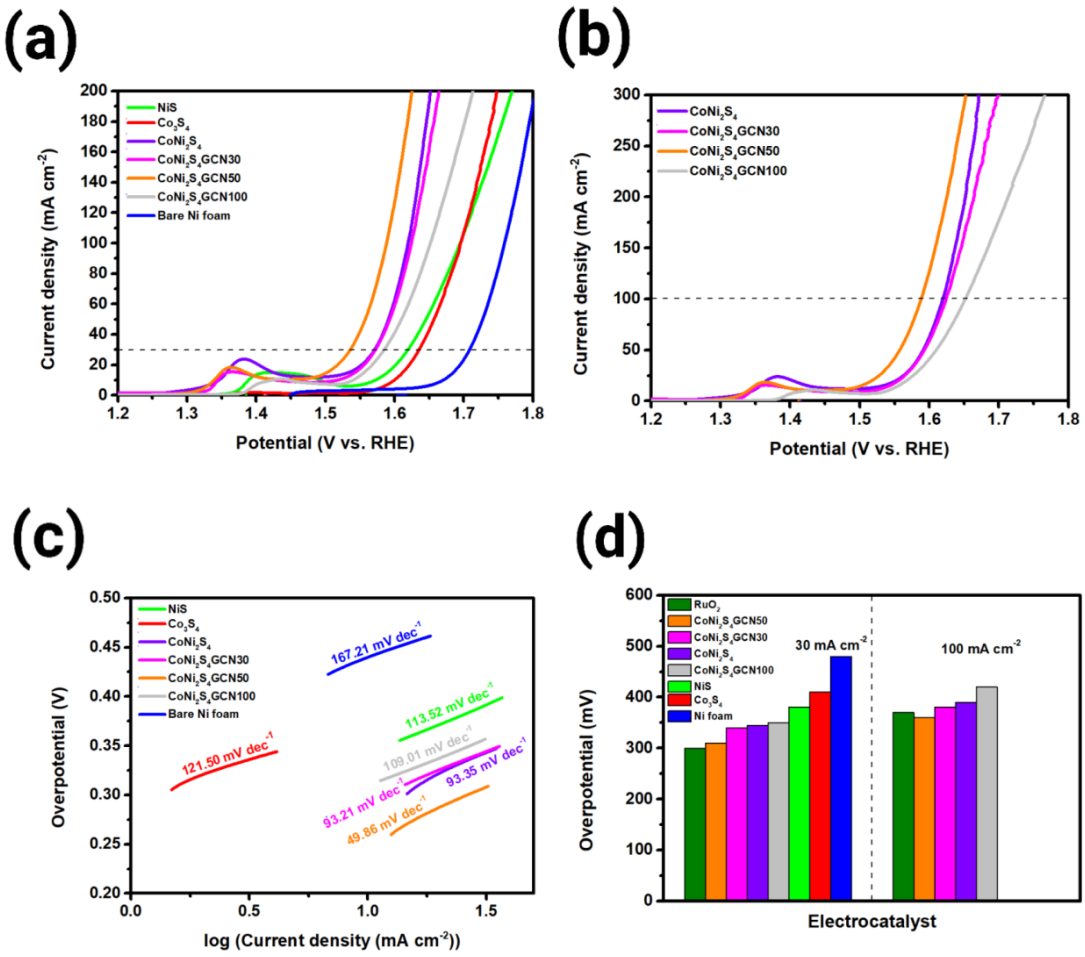

Figure 10. (a) Polarization curves OER for NiS, Co_3S_4, $CoNi_2S_4$, $CoNi_2S_4$GCN30, $CoNi_2S_4$GCN50 and $CoNi_2S_4$GCN100 samples at a scan rate of 5 mV/s in 1M KOH. (b) LSV curves of $CoNi_2S_4$, $CoNi_2S_4$GCN30, $CoNi_2S_4$GCN50 and $CoNi_2S_4$GCN100. (c) Tafel slopes of NiS, Co_3S_4, $CoNi_2S_4$, $CoNi_2S_4$GCN30, $CoNi_2S_4$GCN50 and $CoNi_2S_4$GCN100. (d) Required overpotential at 10 mA/cm^2 and 100 mA/cm^2.

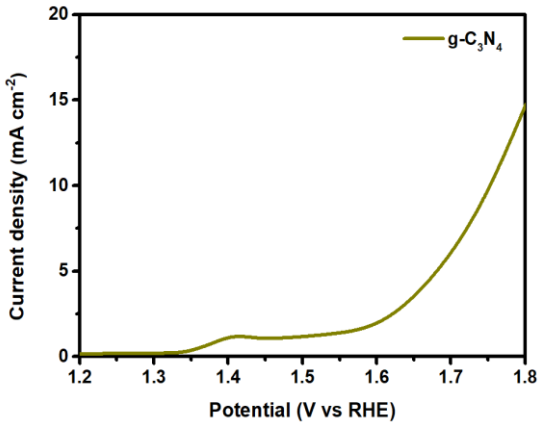

Figure 11. Polarization curve OER of graphitic carbon nitride.

Table 3: Compared OER activity of electrocatalysts

Electrocatalyst	**Over potential**	**Current density**	**Reference**
MOF derived NiCoS	340 mV	30 mA cm^{-2}	[91]
Ferrocene incorporated CoS	350 mV	30 mA cm^{-2}	[92]
WS_2/CoS/carbon materials	390 mV	30 mA cm^{-2}	[93]
CoFe/NiCoS	260 mV and 280 mV	10 mA cm^{-2} and 30 mA cm^{-2}	[94]
NiCoS/CoS on nickel foam	350 mV	30 mA cm^{-2}	[95]
Nickel phosphate/NiO	332 mV	10 mA cm^{-2}	[96]
NiCoS supported on CuO/Cu	290 mV	30 mA cm^{-2}	[97]
$CoNi_2S_4$GCN50	310 mV	30 mA cm^{-2}	This work

4.1.6.2 Hydrogen evolution reaction

The HER activity of all the prepared catalysts was studied in 1M KOH solution and on a three-electrode assembly of Pt mesh, Ag/AgCl and catalysts coated on nickel foam(NF) as a working electrode. For comparison, Platinum mesh and bare nickel foam were also tested under similar conditions. The LSV curves of all the prepared catalysts are depicted in figure 12. g-C_3N_4 on nickel foam has shown very low activity for HER at a current density of 10 mA/cm^2 as shown in figure 13. NiS and Co_3S_4 have shown inferior activity for HER with an onset-potential of 250 mV and 280 mV and over-potential of 280 mV and 290 mV to maintain 10 mA/cm^2 $CoNi_2S_4$ and $CoNi_2S_4$GCN50 have exhibited an onset-potential of 160 mV with an over-potential of 200 mV and 210 mV to 10 mA/cm^2 as shown in figure 12b. $CoNi_2S_4$GCN50 has shown higher activity for HER among all as-prepared catalysts with lower over-potential of 160 mV to attain a current density of 10 mA/cm^2 and with an onset potential of 140 mV revealing the addition of g-C_3N_4 increases the HER activity of $CoNi_2S_4$. Further increasing the g-C_3N_4 concentration in $CoNi_2S_4$ lowers its electrocatalytic activity due to the problems of agglomeration as confirmed from the $CoNi_2S_4$GCN100 HER polarization results, requires over-potential of 215 mV to achieve 10 mA/cm^2 of current density and an onset potential of 140 mV. Introducing g-C_3N_4 in higher concentrations decreases the active sites of $CoNi_2S_4$. These results confirmed the successful fabrication of $CoNi_2S_4$GCN50, implying that 50 mg g-C_3N_4 exposes more surface area and allows uniform distribution of $CoNi_2S_4$ on graphitic carbon nitride. To gain further knowledge about HER mechanism Tafe slope of all the as-synthesized catalysts is shown in figure 12c.

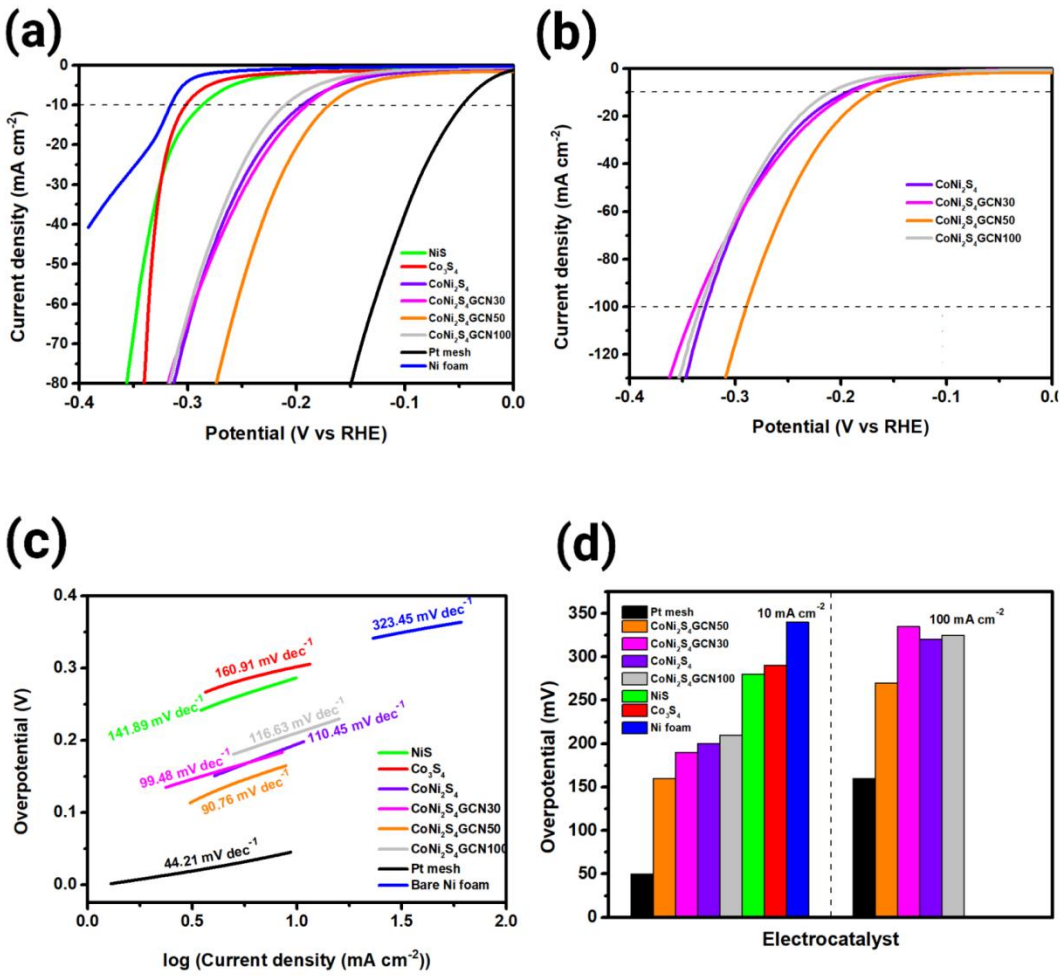

Figure 12. (a) Polarization curves HER for NiS, Co_3S_4, $CoNi_2S_4$, $CoNi_2S_4$GCN30, $CoNi_2S_4$GCN50 and $CoNi_2S_4$GCN100 samples at a scan rate of 5 mV/s in 1M KOH. (b) LSV curves of $CoNi_2S_4$, $CoNi_2S_4$GCN30, $CoNi_2S_4$GCN50 and $CoNi_2S_4$GCN100. (c) Tafel slopes of NiS, Co_3S_4, $CoNi_2S_4$, $CoNi_2S_4$GCN30, $CoNi_2S_4$GCN50 and $CoNi_2S_4$GCN100. (d) Required overpotential at 10 mA/cm^2 and 100 mA/cm^2

HER rate-limiting step is determined from its Tafel slope and smaller Tafel slope depicts higher HER rate. Tafel slope of $CoNi_2S_4$GCN50 (90.76 mV/dec) is lowest among all other catalysts $CoNi_2S_4$ (110.45 mV/dec), $CoNi_2S_4$GCN30 (99.48 mV/dec),$CoNi_2S_4$GCN100 (116.63 mV/dec), NiS (141.89 mV/dec), Co_3S_4 (160.91

mV/dec) and bare nickel foam (323.45 mV/dec). The lower Tafel slope for $CoNi_2S_4$GCN50 (90.76 mV/dec) demonstrates that the rate-determining step is Heyrovsky reaction and Volmer- Heyrovsky reaction is taking place in this electrocatalyst [98]. These results depict that the catalytic activity of $CoNi_2S_4$ enhances by the addition of g-C_3N_4. A comparison with the previous reports is given in table 3.

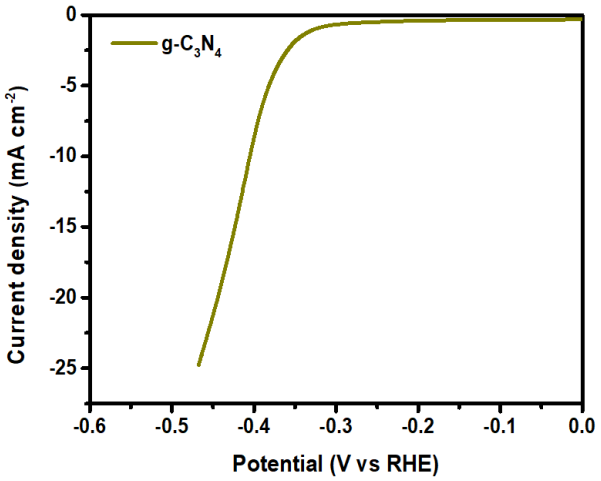

Figure 13. Polarization curve HER of graphitic carbon nitride.

Table 4: Compared HER activity of electrocatalysts

Electrocatalyst	**Over potential**	**Current density**	**Reference**
NiCoS	280 mV	10 mA cm^{-2}	[99]
NiCoS(1:2)	282 mV	10 mA cm^{-2}	[29]
NiCoS nano array	228 mV	10 mA cm^{-2}	[100]
NiS.Cu_5FeS_4	140 mV	10 mA cm^{-2}	[101]
CoO and TiO_2 coupled with CNT and graphitic carbon on MXene nanosheets	367.8 mV	10 mA cm^{-2}	[102]
FeS_2/MoS_2/g-C_3N_4	334 mV	10 mA cm^{-2}	[103]
$CoNi_2S_4$GCN50	160 mV	10 mA cm^{-2}	This work

4.1.6.3 Cyclic Voltammetry

The CV curves of all prepared samples shown in figure 14 and 15 at a scan rate of 5-100 mV/s in 1M KOH electrolyte. A compared cyclic voltammetry of all the as-synthesized samples shown in figure 16, clearly indicates two well-defined redox peaks of all sulfides, suggesting their electroactive nature. Furthermore from the data of this cyclic voltammetry, it can be depicted that the intensity of redox peaks increases on the addition of graphitic carbon nitride to nickel-cobalt sulfide attributing to its enhanced electroactive nature. This can be allocated to the coupling of Co and Ni with C and N [104, 105]. By increasing the scan rate the CV of all samples maintains a constant curve shape suggesting the excellent cyclic stability and smaller resistance of electrocatalysts.

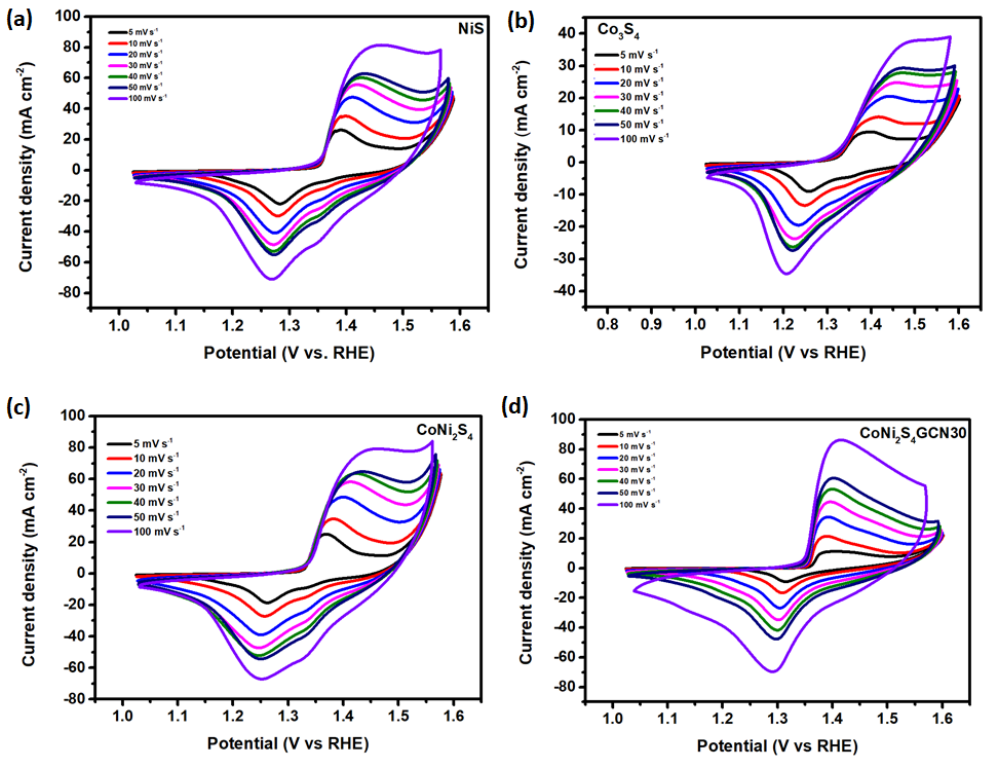

Figure 14. Cyclic voltammetry curve of (a) NiS, (b) Co_3S_4, (c) $CoNi_2S_4$ and (d) $CoNi_2S_4GCN30$

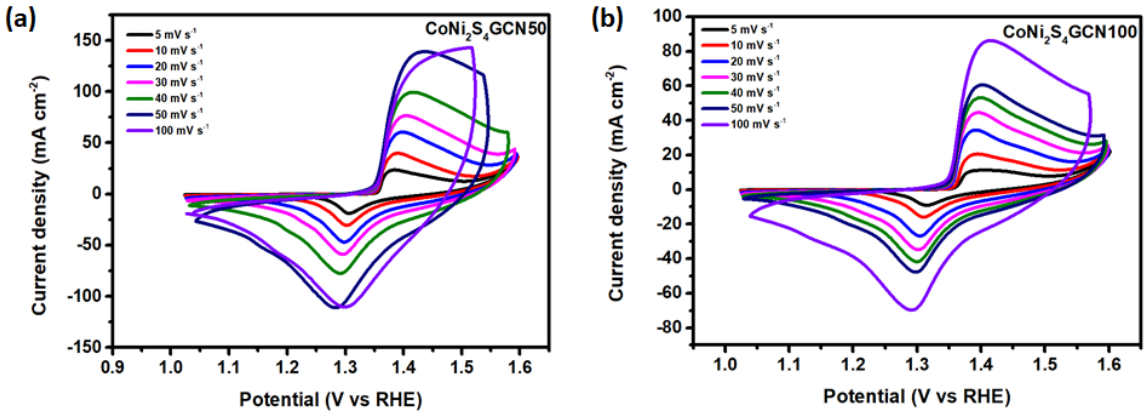

Figure 15. Cyclic voltammetry curves of (a) $CoNi_2S_4GCN50$ and (b) $CoNi_2S_4GCN100$

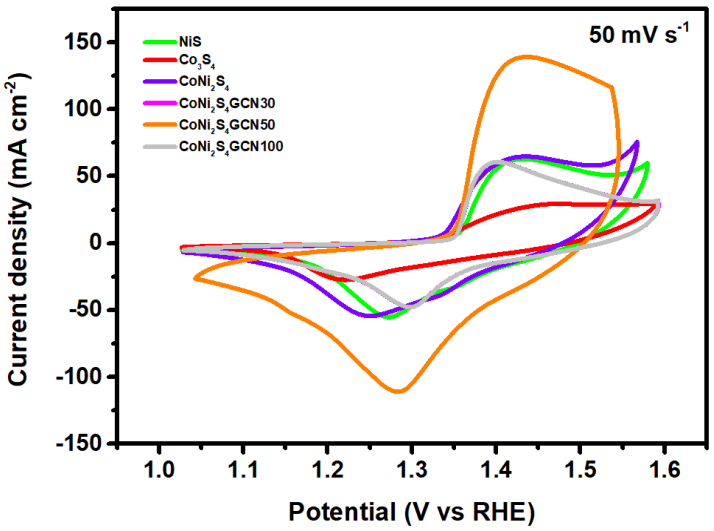

Figure 16. Comparison Cyclic voltammetry curves of NiS, Co_3S_4, $CoNi_2S_4$, $CoNi_2S_4GCN30$, $CoNi_2S_4GCN50$ and $CoNi_2S_4GCN100$ at a scan rate of 50 mV s^{-1}

4.1.6.4 Electrochemical impedance spectroscopy

The kinetics of as-prepared samples was further investigated by EIS measurements in 1M KOH electrolyte shown in figure 17. EIS results indicate the circuit elements, ohmic resistance between electrodes associated with the electrolyte (R_1), polarization resistance (R_2) associated with the charge transfer resistance, C_2 indicates the faradic capacitance and W represents Warburg impedance. The radius of a semi-circle in the Nyquist plot depicts R_2. From the data of table 4, $CoNi_2S_4$GCN50 has shown the least charge transfer resistance (0.11 **Ω)** among all the as-synthesized $CoNi_2S_4$GCN30 (0.384 **Ω**), $CoNi_2S_4$GCN100 (0.481 **Ω**), $CoNi_2S_4$ (0.368 **Ω**), NiS (3.235 **Ω**) and Co_3S_4 (2.322 **Ω**). Therefore, it is logical to argue that C, N bond with Co and NiS are favourable for enhanced electron transfer rate. Lower values R_1 and R_2 reflects higher kinetics for OER and HER. $CoNi_2S_4$ when compared with NiS and Co_3S_4 has the least resistance of electrolyte and lower charge transfer resistance, depicting the synergistic effect of Ni and Co sulfide. Fitting EIS data in an equivalent electric circuit as shown in figure 17b, gives the value of the constant phase element Q for double layer response. However, the adsorption of reaction intermediates is modelled with relevant adsorption capacitance and resistance. This is not just an arbitrary model to fit electrochemical impedance data each value in this model has a clear physical meaning. Randles model fitted in the EIS data indicate the circuit elements, ohmic resistance between electrodes associated with the electrolyte (R_1), polarization resistance (R_2) associated with the charge transfer resistance, Q indicates the CPE value with the units of $mF.s^{a-1}$ and is related to the phase angle of frequency. It is worth mentioning that when a=0 constant phase element behaves as a pure resistor and when a=1, CPE acts as a pure capacitor. The radius of a semi-circle in the Nyquist plot depicts R_2. From the data of table 4, $CoNi_2S_4$GCN50 has shown the least charge transfer resistance (0.384 **Ω)** among all the as-synthesized electrocatalysts. Therefore, it is logical to argue that C, N bond with Co and NiS are favourable for enhanced electron transfer rate. Lower values R_1 and R_2 reflects higher kinetics for OER and HER. $CoNi_2S_4$ when compared with NiS and Co_3S_4 has the least resistance of electrolyte and lower charge transfer resistance, depicting the synergistic effect of Ni and Co sulfide.

Table 5. R_{ct}, C_{dl} and ESCA of NiS, Co_3S_4, $CoNi_2S_4$, $CoNi_2S_4$GCN30, $CoNi_2S_4$GCN50 and $CoNi_2S_4$GCN100.

Electrocatalyst	R_1 (Ω)	R_2 (Ω)	Q (mFs^{a-1})	a	C_{dl} ($mFcm^{-2}$)	ESCA
NiS	0.761	0.111	7.48	0.995	7.464	186.6
Co_3S_4	0.968	5.28	5.33	0.815	7.28	182.3
$CoNi_2S_4$	0.870	0.763	9.41	0.804	13.03	325.7
$CoNi_2S_4$GCN30	0.750	0.863	10.12	0.791	14.49	362.2
$CoNi_2S_4$GCN50	**0.399**	**0.384**	**27.1**	**0.826**	**38.47**	**961.7**
$CoNi_2S_4$GCN100	1.17	10.61	3.54	0.71	5.87	145

To gain more understanding of the kinetics of catalysts, electrocatalytic active surface area (ESCA) is an important parameter to estimate the enhanced catalytic activity of catalysts in a system. BET only measures the physical surface area but the estimation of ESCA is crucial in scheming electrocatalysts for water splitting. Electrochemical double-layer capacitance is employed to estimate the electrocatalytic active surface area (ESCA) of an electrocatalyst. The most commonly employed method for its calculation is by measuring non-faradic current at different scan rates of CV related to the double-layer charging. But as depicted in figure 17a, it is difficult to measure non-faradic current zones as the synthesized materials have shown sharp redox peaks. Another approach of measuring this C_{dl} is by computing the frequency-related impedance of the entire electrochemical cell employing electrochemical impedance spectroscopy [106, 107]. C_{dl} value measured by CV and EIS varies within the range of ±15%. The electrochemical system is estimated within the region of non-faradic response and high frequency by a Randles circuit of EC-lab demo, as depicted in figure 17b. The double-layer capacitance (C_{dl}) of all electrocatalysts was calculated using equation 6 [108].

$$C_{dl} = [Q.[1/R_1+1/R_2]^{a-1}]^{1/a} \qquad \text{(Eq.8)}$$

$CoNi_2S_4$GCN50 has shown the enhanced value of double-layer capacitance depicting the addition of graphitic carbon nitride enhances the catalytic activity of nickel-cobalt sulfide. The electrocatalytic active surface area (ESCA) is commonly estimated using equation 7.

$$ESCA = C_{dl}/C_s \qquad \text{(Eq.9)}$$

Where C_s, the specific capacitance is usually taken as, 0.040 $mFcm^{-2}$ for common electrocatalysts in 1M KOH solution [109]. $CoNi_2S_4$GCN50 has depicted the highest value of ESCA (961.7) in table 1, employing that the electrocatalytic active surface area of nickel cobalt sulfide improves drastically by graphitic carbon nitride addition.

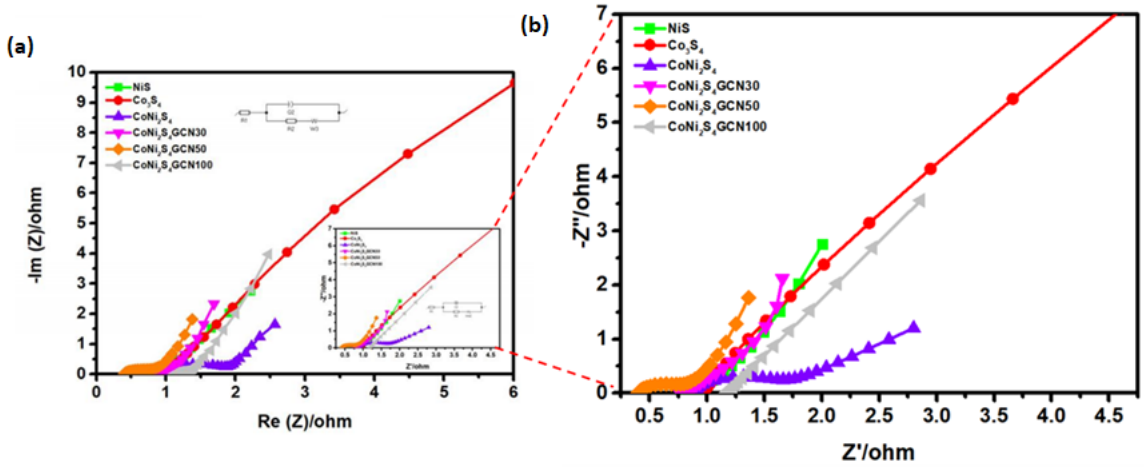

Figure 17. Nyquist plots of NiS, Co_3S_4, $CoNi_2S_4$, $CoNi_2S_4$GCN30, $CoNi_2S_4$GCN50 and $CoNi_2S_4$GCN100 at a frequency range of 200 kHz-0.1 Hz.

4.1.6.5 Chronoamperometry

Stability is an important issue which should be taken into consideration while commercializing electrocatalyst for water splitting. $CoNi_2S_4$GCN50 has shown long term stability for 24 hours in figure 18. As expected $CoNi_2S_4$GCN50 depicted excellent activity and has kept 90% of its initial current density after 12 hours of chrono-amperometric responses in 1M KOH solution, higher than [33, 110, 111]

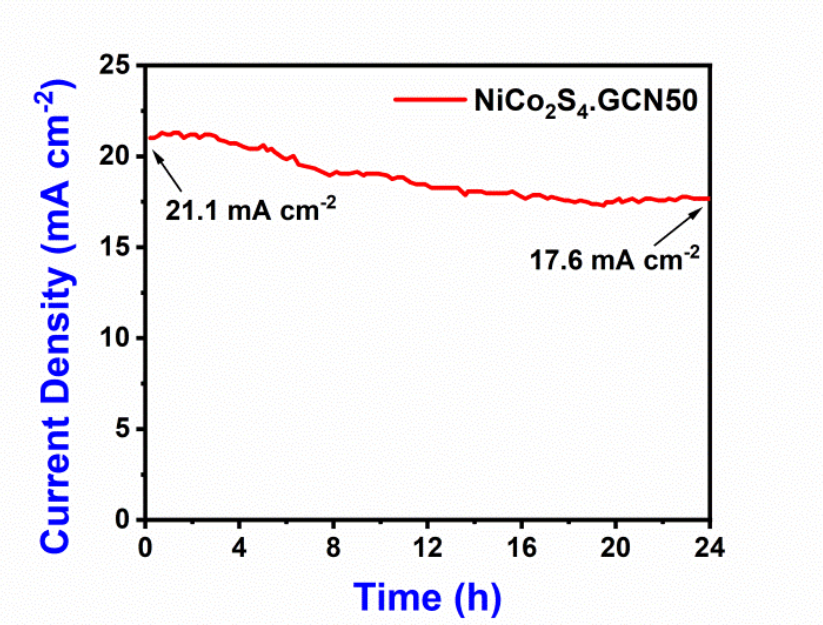

Figure 18. Chronoamperometry curve of $CoNi_2S_4$GCN50 for 24 hours

Table 6: Compared catalytic activity of electrocatalyst for overall water splitting.

Electrocatalyst	**Required potential**	**Current density**	**Reference**
$CuCo_2S_4$	1.66 V	10 mA cm^{-2}	[112]
$NiFeO(OH)/MoS_2$	1.57 V	10 mA cm^{-2}	[113]
Co_9S_8/Ni_3Se_2	1.62 V	10 mA cm^{-2}	[114]
$CoNi_2S_4$GCN50	1.58 V	10 mA cm^{-2}	This work

4.1.6.6 $CoNi_2S_4GCN50$ as electrolyzer for overall water splitting

$CoNi_2S_4GCN50$ in alkaline solution displayed outstanding performance for OER and HER. The bifunctional device was constructed with $CoNi_2S_4GCN50$ as anode and cathode and for comparison two-electrode cell of bare NF (nickel foam) was also investigated under same process conditions shown in figure 19. A cell voltage of 1.58 Volt was required at a current density of 10 mA/cm^2, which is lower than Pt. C ‖ IrO_2 with an electrolysis voltage of 1.81 Volt and other water-splitting devices reported in table 5. The current density of $CoNi_2S_4GCN50$ has shown negligible decrease after 12 hours and produced a large number of easily visible gas bubbles indicating $CoNi_2S_4GCN50$ has formidable performance for overall water splitting with excellent stability in an alkaline media.

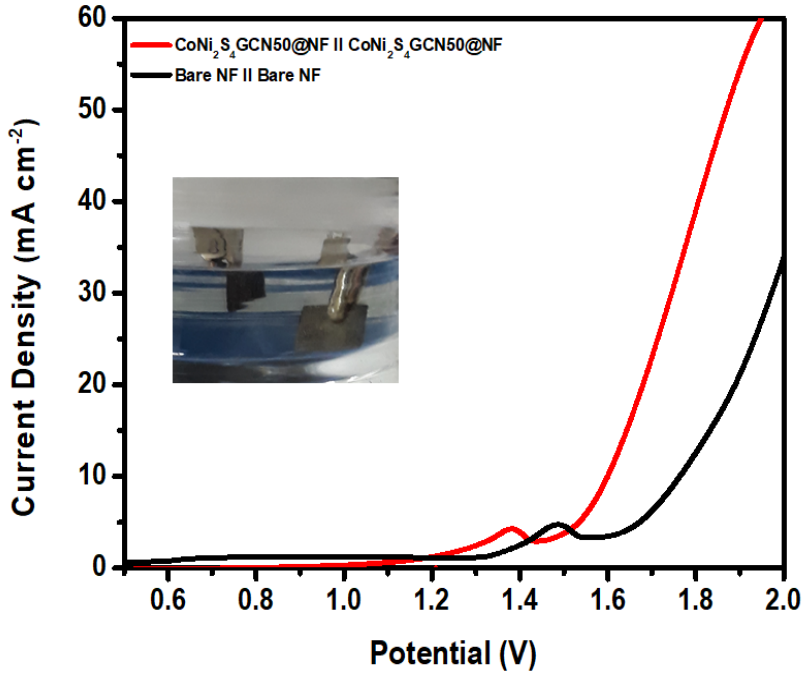

Figure 19. Overall water splitting performance of electrolysis cells: $CoNi_2S_4GCN50$@NF II $CoNi_2S_4GCN50$@NF and Bare NF II Bare NF.

5 Conclusion

The thesis report gives a deep insight into progressive developments done in transition metal sulfides as an electrocatalyst for OER and HER. The main aim of this work is to find low cost, non-precious metal catalyst showing high catalytic activity and stability. Thus, this demand brought nickel-cobalt sulfide quite favourable for effective catalytic properties.

In summary, a hybrid was composed of CoNi2S4 cubic crystals which were covered by a graphitic carbon nitride porous sheet synthesized through the simple hydrothermal method and investigated the activity in alkaline media for OER and HER. $CoNi_2S_4$GCN after optimizing the ratio of graphitic carbon nitride ($CoNi_2S_4$GCN50) at a current density of 100 mA cm^{-2} exhibited low overpotential of 350 mV for OER and an HER overpotential of 150 mV to maintain a 10 mA cm^{-2} current density, respectively. All the experimental results depicted the enhanced OER and HER catalytic activity, due to the C and N-bonds with Co and NiS that induced higher charge transfer rates, enhanced the diffusion of electrolyte and conductivity. The hierarchical petals of $CoNi_2S_4$GCN50 prevented agglomeration and enhanced the active surface area of $CoNi_2S_4$. Furthermore, the structure provided the hierarchy of well-connected nickel-cobalt sulfide and graphitic carbon nitride allowing efficient transfer of electrons and lead to the change in the intermediates binding energy for HER and OER. The bifunctional electrocatalyst required a voltage of 1.58 mV to acquire 10 mA cm^{-2}. This study provides a new approach to design sulfide heterostructure catalyst for electrocatalytic water splitting.

6 Future Recommendations

Despite the great progress made electrocatalysts, some challenging issues remain. On the surface of the cathode, is not only the reason for pH polarization between anode and cathode but it causes alkylation of electrolyte. This enhanced over-potential can be recovered using pH stable electrocatalysts. Due to electrolyte flow and other stresses stability is another important issue for HER electrocatalysts. Furthermore, these nickel and cobalt sulphides can be used as OER catalysts in acidic media. More work needs to be done on these catalysts for OER. Future breakthrough is needed in the structure and design of these electrocatalysts.

References

[1]. Ellabban, O., H. Abu-Rub, and F. Blaabjerg, *Renewable energy resources: Current status, future prospects and their enabling technology.* Renewable and Sustainable Energy Reviews, 2014. **39**: p. 748-764.

[2]. Lewis, N.S. and D.G.J.P.o.t.N.A.o.S. Nocera, *Powering the planet: Chemical challenges in solar energy utilization.* 2006. **103**(43): p. 15729-15735.

[3]. Seh, Z.W., et al., *Combining theory and experiment in electrocatalysis: Insights into materials design.* 2017. **355**(6321).

[4]. Campos-Martin, J.M., G. Blanco-Brieva, and J.L.J.A.C.I.E. Fierro, *Hydrogen peroxide synthesis: an outlook beyond the anthraquinone process.* 2006. **45**(42): p. 6962-6984.

[5]. Mayyas, A., M. Wei, and G. Levis, *Hydrogen as a long-term, large-scale energy storage solution when coupled with renewable energy sources or grids with dynamic electricity pricing schemes.* International Journal of Hydrogen Energy, 2020. **45**(33): p. 16311-16325.

[6]. Tiwari, D.K., et al., *Water Splitting by Using Electrochemical Properties of Material*, in *Water Remediation*. 2018. p. 135-153.

[7]. You, B. and Y. Sun, *Innovative Strategies for Electrocatalytic Water Splitting.* Acc Chem Res, 2018. **51**(7): p. 1571-1580.

[8]. S. Anantharaj, S.R.E., K. Karthick, *Precision and correctness in the evaluation of electrocatalytic water splitting: revisiting activity parameters with a critical assessment.* royal society of chemistry, 2018.

[9]. Wei Li, N.J., Bo Hu, Tanner B. Hanson, T. Leo Liu,Yujie Sun, *Electrolyzer Design for Flexible Decoupled Water Splitting and Organic Upgrading with Electron Reservoirs.* 2018.

[10]. Li, J. and G. Zheng, *One-Dimensional Earth-Abundant Nanomaterials for Water-Splitting Electrocatalysts.* Adv Sci (Weinh), 2017. **4**(3): p. 1600380.

[11]. Bu, L., et al., *Surface engineering of hierarchical platinum-cobalt nanowires for efficient electrocatalysis.* Nat Commun, 2016. **7**: p. 11850.

[12]. Lee, Y., et al., *Synthesis and Activities of Rutile IrO2 and RuO2 Nanoparticles for Oxygen Evolution in Acid and Alkaline Solutions.* J Phys Chem Lett, 2012. **3**(3): p. 399-404.

[13]. Panda, C., et al., *Boosting Electrocatalytic Hydrogen Evolution Activity with a NiPt3@NiS Heteronanostructure Evolved from a Molecular Nickel-Platinum Precursor.* J Am Chem Soc, 2019. **141**(34): p. 13306-13310.

[14]. Kundu, M., G. Singh, and A.M. Svensson, *Co(OH)2@MnO2 nanosheet arrays as hybrid binder-free electrodes for high-performance lithium-ion batteries and supercapacitors.* New Journal of Chemistry, 2019. **43**(3): p. 1257-1266.

[15]. Zahra, R., et al., *A review on nickel cobalt sulphide and their hybrids: Earth abundant, pH stable electro-catalyst for hydrogen evolution reaction.* International Journal of Hydrogen Energy, 2020. **45**(46): p. 24518-24543.

[16]. Rabi, O., et al., *An inclusive review on the synthesis of molybdenum carbide and its hybrids as catalyst for electrochemical water splitting.* Molecular Catalysis, 2020. **494**.

[17]. Ray, C., et al., *Stacked Porous Iron-Doped Nickel Cobalt Phosphide Nanoparticle: An Efficient and Stable Water Splitting Electrocatalyst.* ACS Sustainable Chemistry & Engineering, 2018. **6**(5): p. 6146-6156.

[18]. Wang, Y., et al., *3 D Porous Nickel-Cobalt Nitrides Supported on Nickel Foam as Efficient Electrocatalysts for Overall Water Splitting.* ChemSusChem, 2017. **10**(21): p. 4170-4177.

[19]. Shit, S., et al., *Cobalt Sulfide/Nickel Sulfide Heterostructure Directly Grown on Nickel Foam: An Efficient and Durable Electrocatalyst for Overall Water Splitting Application.* ACS Appl Mater Interfaces, 2018. **10**(33): p. 27712-27722.

[20]. Huang, R., et al., *Well-designed cobalt-nickel sulfide microspheres with unique peapod-like structure for overall water splitting.* J Colloid Interface Sci, 2019. **556**: p. 401-410.

[21]. Dong, B., et al., *Urchin-Like Nanorods of Binary NiCoS Supported on Nickel Foam for Electrocatalytic Overall Water Splitting.* Journal of The Electrochemical Society, 2018. **165**(3): p. H102-H108.

[22]. Tiwari, A.P., et al., *Continuous Network of Phase-Tuned Nickel Sulfide Nanostructures for Electrocatalytic Water Splitting.* ACS Applied Nano Materials, 2019. **2**(8): p. 5061-5070.

[23]. Li, X.-X., et al., *In situ formation of consubstantial NiCo2S4 nanorod arrays toward self-standing electrode for high activity supercapacitors and overall water splitting.* Journal of Power Sources, 2018. **402**: p. 116-123.

[24]. Tang, S., et al., *Combining Co3S4 and Ni:Co3S4 nanowires as efficient catalysts for overall water splitting: an experimental and theoretical study.* Nanoscale, 2019. **11**(5): p. 2202-2210.

[25]. Xu, X., et al., *MoS2/NiS heterostructure grown on Nickel Foam as highly efficient bifunctional electrocatalyst for overall water splitting.* International Journal of Hydrogen Energy, 2020. **45**(35): p. 17329-17338.

[26]. Gong, Y., et al., *Crossed NiCo2S4Nanowires Supported on Nickel Foam as a Bifunctional Catalyst for Efficient Overall Water Splitting.* ChemistrySelect, 2019. **4**(4): p. 1180-1187.

[27]. Zhang, D., et al., *Structure-design and synthesis of Nickel-Cobalt-Sulfur arrays on nickel foam for efficient hydrogen evolution.* Journal of Alloys and Compounds, 2019. **785**: p. 468-474.

[28]. Wu, C., et al., *MOF-derived formation of nickel cobalt sulfides with multi-shell hollow structure towards electrocatalytic hydrogen evolution reaction in alkaline media.* 2019. **177**: p. 107252.

[29]. Tie, J., et al., *Controllable synthesis of hierarchical nickel cobalt sulfide with enhanced electrochemical activity.* 2018. **435**: p. 187-194.

[30]. Du, X., W. Lian, and X.J.I.J.o.H.E. Zhang, *Homogeneous core–shell NiCo2S4 nanorods as flexible electrode for overall water splitting.* 2018. **43**(45): p. 20627-20635.

[31]. Wang, D., et al., *CoNi2S4 nanoparticles as highly efficient electrocatalysts for the hydrogen evolution reaction in alkaline media.* 2017. **42**(5): p. 3043-3050.

[32]. Shen, J., et al., *Design and synthesis of three-dimensional needle-like CoNi2S4/CNT/graphene nanocomposite with improved electrochemical properties.* 2016. **42**(7): p. 8120-8127.

[33]. Dai, W., et al., *Flower-like CoNi2S4/Ni3S2 nanosheet clusters on nickel foam as bifunctional electrocatalyst for overall water splitting.* 2020. **844**: p. 156252.

[34]. Jo, W.-K., et al., *Cobalt-coordinated sulfur-doped graphitic carbon nitride on reduced graphene oxide: An efficient metal–(N, S)–C-class bifunctional electrocatalyst for overall water splitting in alkaline media.* 2019. **7**(18): p. 15373-15384.

[35]. Wang, S., et al., *Nanocoral-like composite of nickel selenide nanoparticles anchored on two-dimensional multi-layered graphitic carbon nitride: a highly efficient electrocatalyst for oxygen evolution reaction.* 2019. **243**: p. 463-469.

[36]. Shabnam, L., et al., *Doping reduced graphene oxide and graphitic carbon nitride hybrid for dual functionality: High performance supercapacitance and hydrogen evolution reaction.* 2020. **856**: p. 113503.

[37]. Li, J., et al., *Sulfur and molybdenum Co-doped graphitic carbon nitride as a superior water dissociation electrocatalyst for alkaline hydrogen evolution reaction.* 2020.

[38]. Bhowmik, T., M.K. Kundu, and S.J.A.A.E.M. Barman, *CoFe layered double hydroxide supported on graphitic carbon nitrides: an efficient and durable bifunctional electrocatalyst for oxygen evolution and hydrogen evolution reactions.* 2018. **1**(3): p. 1200-1209.

[39]. Sun, Y., et al., *Electrodeposited cobalt-sulfide catalyst for electrochemical and photoelectrochemical hydrogen generation from water.* J Am Chem Soc, 2013. **135**(47): p. 17699-702.

[40]. Bo You, N.J., Meili Sheng and Yujie Sun, *Microwave vs. solvothermal synthesis of hollow cobalt sulfide nanoprisms for electrocatalytic hydrogen evolution and supercapacitors.* royal society of chemistry, 2015.

[41]. Li, N., et al., *Vertically grown CoS nanosheets on carbon cloth as efficient hydrogen evolution electrocatalysts.* International Journal of Hydrogen Energy, 2017. **42**(15): p. 9914-9921.

[42]. Huang, G., et al., *Synthesis and electrochemical performances of cobalt sulfides/graphene nanocomposite as anode material of Li-ion battery.* Journal of Power Sources, 2013. **235**: p. 122-128.

[43]. C. Ranaveera, Z.W., E. Alqurashi, *Highly stable hollow bifunctional cobalt sulfides for flexible supercapacitor and hydrogen evolution.* royal society of chemistry, 2016.

[44]. Zhang, Y., et al., *Hierarchical Co9S8 hollow microspheres as multifunctional electrocatalysts for oxygen reduction, oxygen evolution and hydrogen evolution reactions.* Electrochimica Acta, 2017. **246**: p. 380-390.

[45]. Ma, Q., et al., *Identifying the electrocatalytic sites of nickel disulfide in alkaline hydrogen evolution reaction.* Nano Energy, 2017. **41**: p. 148-153.

[46]. Nan Jiang, M.S., Bo You,, *Nickel sulfides for electrocatalytic hydrogen evolution under alkaline conditions: a case study of crystalline NiS, NiS2, and Ni3S2 nanoparticles.* royal society of chemistry, 2015.

[47]. Tiwari, D.K., et al., *Water Splitting by Using Electrochemical Properties of Material.* 2018: p. 135-153.

[48]. Dubouis, N. and A. Grimaud, *The hydrogen evolution reaction: from material to interfacial descriptors.* Chem Sci, 2019. **10**(40): p. 9165-9181.

[49]. Michelle P. Browne, Z.k.S.a.M.P., *Layered and two dimensional metal oxides for electrochemical energy conversion.* royal society of chemistry, 2019.

[50]. Sultan, S., et al., *Single Atoms and Clusters Based Nanomaterials for Hydrogen Evolution, Oxygen Evolution Reactions, and Full Water Splitting.* Advanced Energy Materials, 2019. **9**(22): p. 1900624.

[51]. Laursen, A.B., et al., *Electrochemical Hydrogen Evolution: Sabatier's Principle and the Volcano Plot.* Journal of Chemical Education, 2012. **89**(12): p. 1595-1599.

[52]. Suen, N.-T., et al., *Electrocatalysis for the oxygen evolution reaction: recent development and future perspectives.* 2017. **46**(2): p. 337-365.

[53]. Guofa Dong, M.F., Senpo Yip, *Insight into the Electrochemical Activation of Carbon-Based Cathodes for Hydrogen Evolution Reaction.* Journals of material chemistry A, 2015.

[54]. Vrubel, H., et al., *Revealing and accelerating slow electron transport in amorphous molybdenum sulphide particles for hydrogen evolution reaction.* Chem Commun (Camb), 2013. **49**(79): p. 8985-7.

[55]. Xu, Y.-h., G.-r. He, and X.-l. Wang, *Hydrogen evolution reaction on the AB5 metal hydride electrode.* International Journal of Hydrogen Energy, 2003. **28**(9): p. 961-965.

[56]. Wang, Z., et al., *Electrocatalytic hydrogen evolution on iron-cobalt nanoparticles encapsulated in nitrogenated carbon nanotube.* International Journal of Hydrogen Energy, 2019. **44**(31): p. 16478-16486.

[57]. Tran, P.D., et al., *Novel cobalt/nickel–tungsten-sulfide catalysts for electrocatalytic hydrogen generation from water.* Energy & Environmental Science, 2013. **6**(8): p. 2452.

[58]. Jiang, N., et al., *Study on Ni–Fe–C cathode for hydrogen evolution from seawater electrolysis.* International Journal of Hydrogen Energy, 2010. **35**(15): p. 8056-8062.

[59]. Tian, J., et al., *Self-supported nanoporous cobalt phosphide nanowire arrays: an efficient 3D hydrogen-evolving cathode over the wide range of pH 0-14.* J Am Chem Soc, 2014. **136**(21): p. 7587-90.

[60]. Peng, S., et al., *Cobalt sulfide nanosheet/graphene/carbon nanotube nanocomposites as flexible electrodes for hydrogen evolution.* Angew Chem Int Ed Engl, 2014. **53**(46): p. 12594-9.

[61]. Zhang, H., et al., *Highly Crystallized Cubic Cattierite CoS 2 for Electrochemically Hydrogen Evolution over Wide pH Range from 0 to 14.* Electrochimica Acta, 2014. **148**: p. 170-174.

[62]. Bigi, J.P., et al., *Electrocatalytic reduction of protons to hydrogen by a water-compatible cobalt polypyridyl platform.* Chem Commun (Camb), 2010. **46**(6): p. 958-60.

[63]. Nippe, M., et al., *Catalytic proton reduction with transition metal complexes of the redox-active ligand bpy2PYMe.* Chemical Science, 2013. **4**(10): p. 3934.

[64]. Tang, C., et al., *NiS2 nanosheets array grown on carbon cloth as an efficient 3D hydrogen evolution cathode.* Electrochimica Acta, 2015. **153**: p. 508-514.

[65]. Zongping Chen, W.R., Libo Gao, Bilu Liu, *Three-dimensional flexible and conductive interconnected graphene networks grown by chemical vapour deposition.* Nature materials, 2011.

[66]. Chen, Y.Z., et al., *From Bimetallic Metal-Organic Framework to Porous Carbon: High Surface Area and Multicomponent Active Dopants for Excellent Electrocatalysis.* Adv Mater, 2015. **27**(34): p. 5010-6.

[67]. Chen, B., et al., *Metal-organic-framework-derived bi-metallic sulfide on N, S-codoped porous carbon nanocomposites as multifunctional electrocatalysts.* Journal of Power Sources, 2016. **334**: p. 112-119.

[68]. Bowei Zhang, G.Y., Chaojiang Li,, *Phase controllable fabrication of zinc cobalt sulfide hollow polyhedrons as high-performance electrocatalysts for the hydrogen evolution reaction.* royal society of chemistry, 2018.

[69]. Cui, Y., et al., *High performance electrocatalysis for hydrogen evolution reaction using nickel-doped CoS2 nanostructures: experimental and DFT insights.* Electrochimica Acta, 2017. **228**: p. 428-435.

[70]. Jiang, Y., et al., *Nickel Cobalt Sulfide Double-Shelled Hollow Nanospheres as Superior Bifunctional Electrocatalysts for Photovoltaics and Alkaline Hydrogen Evolution.* ACS Appl Mater Interfaces, 2018. **10**(11): p. 9379-9389.

[71]. Zhou, X., et al., *Symmetrical synergy of hybrid Co9S8-MoSx electrocatalysts for hydrogen evolution reaction.* Nano Energy, 2017. **32**: p. 470-478.

[72]. Liu, Z.-Z., et al., *Triple Ni-Co-Mo metal sulfides with one-dimensional and hierarchical nanostructures towards highly efficient hydrogen evolution reaction.* Journal of Catalysis, 2018. **361**: p. 204-213.

[73]. Han, Q., et al., *Electrochemical evolution of hydrogen on composite La–Ni–Al/Ni–S alloy film in water electrolysis.* Renewable Energy, 2010. **35**(12): p. 2627-2631.

[74]. Tang, C., et al., *Ni3S2 nanosheets array supported on Ni foam: A novel efficient three-dimensional hydrogen-evolving electrocatalyst in both neutral and basic solutions.* International Journal of Hydrogen Energy, 2015. **40**(14): p. 4727-4732.

[75]. Ge, Y., et al., *Facile synthesis of CoNi 2 S 4 and CuCo 2 S 4 with different morphologies as prominent catalysts for hydrogen evolution reaction.* International Journal of Hydrogen Energy, 2016. **41**(44): p. 19847-19854.

[76]. Shao, L., et al., *Low-cost and highly efficient CoMoS4/NiMoS4-based electrocatalysts for hydrogen evolution reactions over a wide pH range.* Electrochimica Acta, 2016. **213**: p. 236-243.

[77]. Yu, X.Y., et al., *Formation of Ni-Co-MoS2 Nanoboxes with Enhanced Electrocatalytic Activity for Hydrogen Evolution.* Adv Mater, 2016. **28**(40): p. 9006-9011.

[78]. Irshad, A. and N. Munichandraiah, *Electrodeposited Nickel-Cobalt-Sulfide Catalyst for the Hydrogen Evolution Reaction.* ACS Appl Mater Interfaces, 2017. **9**(23): p. 19746-19755.

[79]. Liu, H., et al., *Heteromorphic NiCo2S4/Ni3S2/Ni Foam as a Self-Standing Electrode for Hydrogen Evolution Reaction in Alkaline Solution.* ACS Appl Mater Interfaces, 2018. **10**(13): p. 10890-10897.

[80]. Li, X., et al., *Preparation and characterization of graphitic carbon nitride through pyrolysis of melamine.* 2009. **94**(2): p. 387-392.

[81]. Zhai, H.-S., L. Cao, and X.-H.J.C.C.L. Xia, *Synthesis of graphitic carbon nitride through pyrolysis of melamine and its electrocatalysis for oxygen reduction reaction.* 2013. **24**(2): p. 103-106.

[82]. Fina, F., et al., *Structural investigation of graphitic carbon nitride via XRD and neutron diffraction.* 2015. **27**(7): p. 2612-2618.

[83]. Li, Q., et al., *High efficiency photocatalysis for pollutant degradation with MoS2/C3N4 heterostructures.* 2014. **30**(29): p. 8965-8972.

[84]. Chen, Z., et al., *In situ formation of cobalt nitrides/graphitic carbon composites as efficient bifunctional electrocatalysts for overall water splitting.* 2018. **10**(8): p. 7134-7144.

[85]. Wang, H., et al., *Structural distortion in graphitic-C 3 N 4 realizing an efficient photoreactivity.* 2015. **7**(12): p. 5152-5156.

[86]. Xia, C., et al., *Is NiCo2S4 really a semiconductor?* 2015. **27**(19): p. 6482-6485.

[87]. Shen, J., et al., *CoNi2S4-Graphene-2D-MoSe2 as an Advanced Electrode Material for Supercapacitors.* 2016. **6**(13): p. 1600341.

[88]. Teo, E.Y.L., et al., *One-step production of pyrene-1-boronic acid functionalized graphene for dopamine detection.* 2019. **231**: p. 286-291.

[89]. Gao, Z., et al., *Enhanced cycleability of faradic CoNi2S4 electrode by reduced graphene oxide coating for efficient asymmetric supercapacitor.* 2018. **281**: p. 394-404.

[90]. Luo, P., et al., *Targeted synthesis of unique nickel sulfide (NiS, NiS2) microarchitectures and the applications for the enhanced water splitting system.* 2017. **9**(3): p. 2500-2508.

[91]. Yu, Z., et al., *MOF-directed templating synthesis of hollow nickel-cobalt sulfide with enhanced electrocatalytic activity for oxygen evolution.* 2018. **43**(18): p. 8815-8823.

[92]. Thangasamy, P., et al., *Ferrocene-Incorporated Cobalt Sulfide Nanoarchitecture for Superior Oxygen Evolution Reaction.* 2020. **16**(31): p. 2001665.

[93]. Huang, Z., et al., *Polyoxometallates@ zeolitic-imidazolate-framework derived bimetallic tungsten-cobalt sulfide/porous carbon nanocomposites as efficient bifunctional electrocatalysts for hydrogen and oxygen evolution.* 2020. **330**: p. 135335.

[94]. Hafezi Kahnamouei, M., S.J.A.a.m. Shahrokhian, and interfaces, *Mesoporous Nanostructured Composite Derived from Thermal Treatment CoFe Prussian Blue Analogue Cages and Electrodeposited NiCo-S as an Efficient Electrocatalyst for an Oxygen Evolution Reaction.* 2020. **12**(14): p. 16250-16263.

[95]. Adhikari, S., Y. Kwon, and D.-H.J.C.E.J. Kim, *Three-dimensional core–shell structured NiCo2O4@ CoS/Ni-Foam electrocatalyst for oxygen evolution reaction and electrocatalytic oxidation of urea.* 2020. **402**: p. 126192.

[96]. Bhanja, P., et al., *Microporous nickel phosphonate derived heteroatom doped nickel oxide and nickel phosphide: Efficient electrocatalysts for oxygen evolution reaction.* 2020. **405**: p. 126803.

[97]. Lu, M., et al., *Hierarchical nickel cobalt sulfide nanosheet arrays supported on CuO/Cu hybrid foams as a rationally designed core–shell dendrite electrocatalyst for an efficient oxygen evolution reaction.* 2020. **4**(8): p. 4039-4045.

[98]. Shinagawa, T., A.T. Garcia-Esparza, and K.J.S.r. Takanabe, *Insight on Tafel slopes from a microkinetic analysis of aqueous electrocatalysis for energy conversion.* 2015. **5**(1): p. 1-21.

[99]. Irshad, A., N.J.A.a.m. Munichandraiah, and interfaces, *Electrodeposited nickel–cobalt–sulfide catalyst for the hydrogen evolution reaction.* 2017. **9**(23): p. 19746-19755.

[100]. Zhang, D., et al., *Structure-design and synthesis of Nickel-Cobalt-Sulfur arrays on nickel foam for efficient hydrogen evolution.* 2019. **785**: p. 468-474.

[101]. Yuan, F., et al., *Coupling interface structure in NixS/Cu5FeS4 hybrid with enhanced electrocatalytic activity for alkaline hydrogen evolution reaction.* 2020. **578**: p. 668-676.

[102]. He, L., et al., *Cobalt oxide doped with titanium dioxide and embedded with carbon nanotubes and graphene-like nanosheets for efficient trifunctional electrocatalyst of hydrogen evolution, oxygen reduction, and oxygen evolution reaction.* Journal of Power Sources, 2019. **414**: p. 333-344.

[103]. Li, Y., et al., *FeS2 bridging function to enhance charge transfer between MoS2 and g–C3N4 for efficient hydrogen evolution reaction.* 2020: p. 127804.

[104]. He, G., et al., *S, N-Co-doped graphene-nickel cobalt sulfide aerogel: improved energy storage and electrocatalytic performance.* 2017. **4**(1): p. 1600214.

[105]. Jin, F., et al., *Synthesis of Hierarchical Porous Ni1.5Co1.5S4/g-C3N4 Composite for Supercapacitor with Excellent Cycle Stability.* Nanomaterials (Basel), 2020. **10**(9).

[106]. Orazem, M.E. and B.J.N.J. Tribollet, *Electrochemical impedance spectroscopy.* 2008: p. 383-389.

[107]. Brug, G., et al., *The analysis of electrode impedances complicated by the presence of a constant phase element.* 1984. **176**(1-2): p. 275-295.

[108]. McCrory, C.C., et al., *Benchmarking heterogeneous electrocatalysts for the oxygen evolution reaction.* J Am Chem Soc, 2013. **135**(45): p. 16977-87.

[109]. McCrory, C.C., et al., *Benchmarking hydrogen evolving reaction and oxygen evolving reaction electrocatalysts for solar water splitting devices.* 2015. **137**(13): p. 4347-4357.

[110]. Liu, X., et al., *Hybrid structured CoNi 2 S 4/Ni 3 S 2 nanowires with multifunctional performance for hybrid capacitor electrodes and overall water splitting.* 2020. **10**(55): p. 33428-33435.

[111]. Ranjith, K.S., et al., *Ultrathin rGO-wrapped free-standing bimetallic CoNi2S4-carbon nanofibers: an efficient and robust bifunctional electrocatalyst for water splitting.* 2020. **31**(27): p. 275402.

[112]. Zequine, C., et al., *Effect of solvent for tailoring the nanomorphology of multinary CuCo2S4 for overall water splitting and energy storage.* 2019. **784**: p. 1-7.

[113]. Zhou, F., et al., *The electrochemical overall water splitting promoted by MoS2 in coupled nickel–iron (oxy) hydride/molybdenum sulfide/graphene composite.* 2020. **397**: p. 125454.

[114]. Hou, Y., et al., *Integrated hierarchical cobalt sulfide/nickel selenide hybrid nanosheets as an efficient three-dimensional electrode for electrochemical and photoelectrochemical water splitting.* 2017. **17**(7): p. 4202-4209.